Thesis Report

On

NUMERICAL ANALYSIS OF STEREOLITHOGRAPHY PROCESS USING THE FINITE ELEMENT METHOD

Submitted in the partial fulfillment of requirement for the award of the degree of

MASTER OF ENGINEERING

IN

CAD/CAM & ROBOTICS

Submitted by

PARVEEN SHARMA
Roll No. 80681014

Under the guidance of

Mr. P.S. RAO
Lecturer
NITTTR, Chandigarh

Mr. J.S. SAINI
Lecturer
Thapar University, Patiala

Mechanical Engineering Department
THAPAR UNIVERSITY
PATIALA-147004

JUNE - 2008

Certificate

I hereby certify that the work which is being presented in the thesis entitled, ***"Numerical Analysis Of Stereolithography Processes Using The Finite Element Method",*** *in partial fulfillment of the requirements for the award of degree of* ***Master of Engineering in Mechanical Engineering*** *with specialization in* ***CAD/CAM & ROBOTICS*** *at* ***Thapar University****, Patiala, is an authentic record of my own work carried out under the supervision of* ***Mr. P.S. Rao (Lecturer, MED, NITTTR, Chandigarh)*** *and* ***Mr. J.S. Saini****,* ***(Lecturer, MED, Thapar University, Patiala (Punjab))*** *and refers other researcher's works which are duly listed in the reference section.*

The matter embodied in this thesis has not been submitted for the award of any other degree of this or any other university.

PARVEEN SHARMA

This is to certify that the above statement made by the candidate is correct and true to the best of my knowledge.

(Mr. P.S. Rao)
Lecturer, MED
NITTTR,
Chandigarh

(Mr. J.S. Saini)
Lecturer, MED
Thapar University,
Patiala

Countersigned by

(Dr. S.K. MOHAPATRA)
Professor and Head,
Mechanical Engineering Department,
Thapar University,
Patiala-147004

(Dr. R.K. SHARMA)
Dean of Academic Affairs,
Thapar University
Patiala -147004

ACKNOWLEDGEMENTS

Words are often less to revels one's deep regards. With an understanding that work like this can never be the outcome of a single person, I take this opportunity to express my profound sense of gratitude and respect to all those who helped me through the duration of this work.

This work would not have been possible without the encouragement and able guidance of my Supervisors ***Mr. P.S. Rao*** *and* ***Mr. J.S. Saini****. Their enthusiasm and optimism made this experience both rewarding and enjoyable. Most of the novel ideas and solutions in this work are the result of our numerous stimulating discussions. Their feedback and editorial comments were also invaluable for the writing of this thesis. I am grateful to* ***Dr. S.K. Mohapatra****, Prof. & Head, MED for providing the facilities for the completion of the work.*

I take pride of myself being son of ideal parents for their everlasting desire, sacrifice, affectionate blessings and help, without which it would not have been possible for me to complete my studies.

At last, I would like to thank to all the members and employees of Mechanical Engineering Department, Thapar University, Patiala for their everlasting support.

Parveen Sharma

Roll No.:80681014

ABSTRACT

In present highly competitive environment need for better design features along with reduced costing has become very important. Rapid Prototyping also referred to as solid free-form manufacturing, computer automated manufacturing, and layered manufacturing has obvious use as a vehicle for visualization. In addition, RP models can be used for testing, such as when an airfoil shape is put into a wind tunnel. Rapid tooling arises from rapid prototyping, such as silicone rubber molds and investment casts. Rapid manufacturing arises from rapid prototyping to use rapid prototyping systems to directly produce parts which are functional end-use item with the advantage that there is no need for tooling.

The rapid prototyping (RP) process is the fastest and most feasible method for prototype construction. However, with the use of any material or build method the phenomenon of volume shrinkage is unavoidable. It is known that volume shrinkage and curl distortion are the major causes that lead to poor accuracy of the built prototype. Subsequently, in order to improve the precision of dimension and volume shrinkage, more expensive equipment is used on the market. Also, it is expensive and inefficient to obtain better process parameters through trail and error in the RP process. In order to improve the precision of dimension, reduce the processing cost and the frequency of trail and error, this study first induces the concept of computer aided engineering (CAE) into the processing of RP, which uses a finite element simulation code to simulate the photopolymerization process, so as to obtain the distortion data. Besides, it is believed that this research method can be promoted to other materials or build methods in RP fabrication.

INDEX

LIST OF FIGURES

LIST OF TABLES

NOMENECLATURE

E	Elastic modulus
G	Shear modulus
J	Jacobien matrix
J^{-1}	Inverse of Jacobien matrix
det J	Determinant of Jacobian matrix
k	Volume modulus
n	Number of nodes
N_i	Shape function
t	Thickness
$\dot{\mathrm{T}}$	Increment in temperature
t_G, t_k	Slack time
V	Volume of the reaction area
x_i, y_i, z_i	Coordinates of the nodes of elements of the prototype
ε_i , η_i, ρ_i	General co-ordinates of eight noded element
η_G	Viscous coefficient in the shear deformation
η_k	Viscous coefficient in the volume deformation relatively
σ_m	Mean stress
σ'	Deviatoric stress
$\dot{\varepsilon}_k$	Volume strain rate
$[\mathrm{B}]$	Strain rate–velocity matrix
$[\mathrm{B}]^{\mathrm{T}}$	Transpose of the matrix $[\mathrm{B}]$
$[B]_{x,y,z}$	Strain rate–velocity matrix matrix in ε , η , ρ coordinates;
$[B]_{\varepsilon,\eta,\rho}$	Strain rate–velocity matrix matrix in ε , η , ρ co-ordinates
$[C^e]$	Elastic flexibility matrix

$\left[D^e\right]$	Elastic stress-strain matrix
$\left[Fglobal\right]$	Force matrix
$\left\{\dot{\mathrm{f}}\right\}$	Increment in the effective nodal force
$\left[K\right]$	Stiffness matrix
$\left[Kglobal\right]$	Global stiffness matrix
$\left[t^{\eta\kappa}\right]$	Slack time matrix
$\left[u\right]$	Displacement matrix
$\left\{\dot{\mathrm{u}}\right\}$	Increment in nodal displacement
$\left\{\dot{\sigma}\right\}$	Stress rate matrix
$\{\sigma\}$	Nodal viscous stress matrix
$\left\{\dot{\varepsilon}\right\}$	Euler strain rate matrix
$\left\{\dot{\varepsilon}^e\right\}$	Elastic strain rate matrix
$\left\{\dot{\varepsilon}^T\right\}$	Thermal strain rate matrix
$\left\{\dot{\varepsilon}^V\right\}$	Viscous strain rate matrix
$\left\{\dot{\varepsilon}^\gamma\right\}$	Strain rate caused by cure shrinkage equals $\left\{\Delta\beta(I,t)\right\}$
$\left\{\dot{\varepsilon}^d\right\}$	Component of viscous strain rate in shear component
$\left\{\dot{\varepsilon}^k\right\}$	Component of viscous strain rate in volume component
α	Linear expansion coefficient
μ	Poisson's ratio
$\Delta\beta(I)$	Strain associated with cure shrinkage

CHAPTER-1 INTRODUCTION

1.1 RAPID PROTOTYPING: AN INTRODUCTION

The term rapid prototyping (RP) refers to a class of technologies that can automatically construct physical models from Computer-Aided Design (CAD) data. These "three dimensional printers" allow designers to quickly create tangible prototypes of their designs, rather than just two-dimensional pictures. Such models have numerous uses. They make excellent visual aids for communicating ideas with co-workers or customers. In addition, prototypes can be used for design testing. For example, an aerospace engineer might mount a model of airfoil in a wind tunnel to measure lift and drag forces. Designers have always utilized prototypes and RP allows them to be made faster and less expensively.

The key idea of rapid prototyping technology is based on decomposition of 3-D computer models into thin cross-sectional layers, followed by physically forming the layers and stacking them up "layer by layer."

"Rapid Prototyping (RP) can be defined as a group of techniques used to quickly fabricate a scale model of a part or assembly using three-dimensional computer aided design (CAD) data" **Jacobs [1]**

Rapid Prototyping has also been referred to as solid free-form manufacturing; computer automated manufacturing, and layered manufacturing. RP has obvious use as a vehicle for visualization. In addition, RP models can be used for testing, such as when an airfoil shape is put into a wind tunnel. RP models can be used to create molds for tooling, such as silicone rubber molds and investment casts. In some cases, the RP part can be the final part, but typically the RP material is not strong or accurate enough. When the RP material is suitable, highly convoluted shapes (including parts nested within parts) can be produced because of the nature of RP.

1.2 METHODOLOGY OF RAPID PROTOTYPING [1]

The basic methodology for all current rapid prototyping techniques can be summarized as follows:

- A CAD model is constructed, and then converted to STL format. The resolution can be set to minimize stair stepping.
- The RP machine processes the STL file by creating sliced layers of the model.
- The first layer of the physical model is created. The model is then lowered by the thickness of the next layer, and the process is repeated until completion of the model.
- The model and any supports are removed. The surface of the model is then finished and cleaned.

1.2.1 The CAD Model

There are many different CAD packages capable of producing an STL file. For rapid prototyping it is essential that parts are complete and have continuity, i.e. the part to be built must be represented as closed surfaces that unambiguously define an enclosed volume. A solid modeler defines a mass having an interior that is completely enclosed and is filled matter. Parts are always complete and have continuity when defined by a solid modeler. A surface modeler builds a number of mathematical patches or surfaces that, when joined together, form the desired part. Since there is no defined association between these surfaces, it is possible to have gaps, discontinuities or even completely missing surfaces. To use a surface modeler for rapid prototyping, the model must be 'fully surfaced', i.e. it must have a closed surface that completely defines an enclosed volume and the inside, outside and boundary of the part must be specified. **Figure 1.1** shows a badly modeled part with overlapping surfaces.

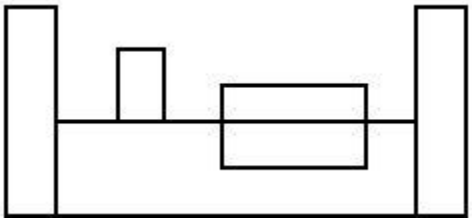

Figure 1.1 Badly modeled part

Figure 1.2 shows a well modeled part with one integral surface.

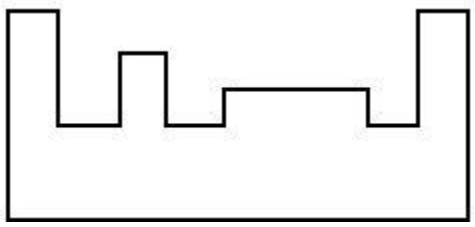

Figure 1.2 Well modeled part

1.2.2 The STL File

The standard file format for rapid prototyping is called STL (Standard Triangulation Language), where the shape of the object is defined by a mesh of tiny triangles laid over the surfaces. The triangles must meet up exactly with each other, without gaps or overlaps, if the object is to be built successfully. The "slice files" which are used to build each individual layer are calculated from the STL file, and if there are any gaps between the triangles, then the edges of the slices are not properly defined.

STL is a standard output format from most CAD (computer-aided design) software, and the number of triangles used can be user-defined. Commonly the translation from the modeling format to STL leaves a few flaws, and so the integrity of STL files is usually checked using special software before the files are used to build an object. Small errors can be corrected automatically, but big faults or ambiguities may need "repairing" by an engineer. **Figure 1.3** shows a sliced model using STL.

When creating an STL file from CAD, the resolution (also known as Tolerance, Chord Height or Facet Deviation) can be specified. Under-faceted STL files will affect the accuracy and may affect the appearance of the part. Over-faceted STL files will increase the time it takes to prepare the part, without improving the quality. There is therefore an optimum resolution for the STL file to give the best accuracy in the smallest file. The resolution is best set between 0.01 mm and 0.05 mm and the overall binary file size should not normally be more than 5 Mbytes.

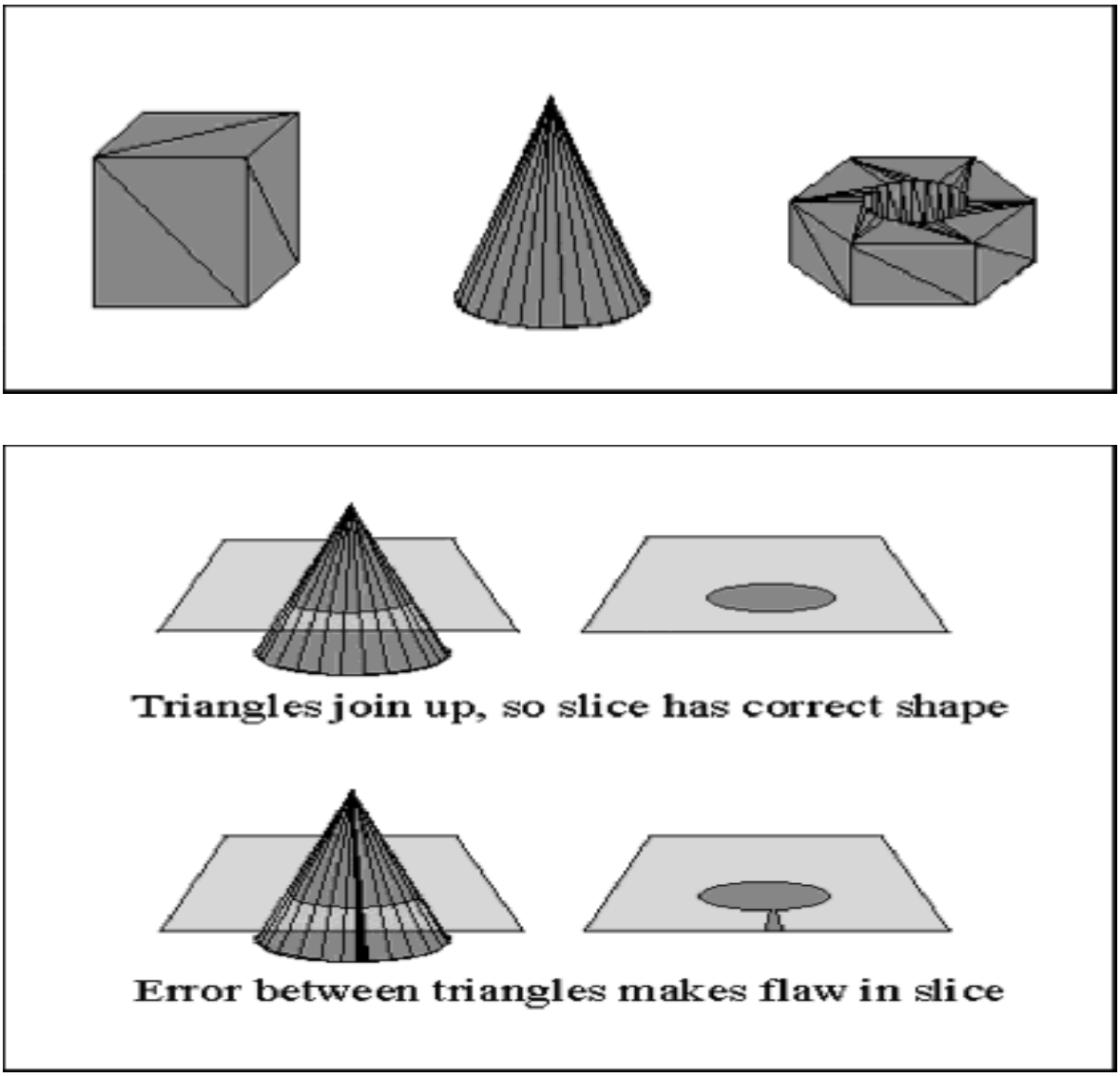

Figure 1.3 A sliced model using STL

Improvements in rapid prototyping technology allow very accurate slice thicknesses, as low as 50 microns, to be achieved. As layers are of finite thickness, small degrees of errors can be tolerated within the Z axis. The final build process requires the merging of multiple STL files to produce the final build file and the building of the component can begin.

1.3 RAPID PROTOTYPING TECHNOLOGIES

Rapid Prototyping Technologies are classified as:

- **Liquid Based Rapid Prototyping Systems**
  - Stereolithography
  - Solid Ground Curing
- **Solid Based Rapid Prototyping Systems**
  - Laminated Object Manufacturing
  - Fused Deposition Modeling
- **Powder Based Rapid Prototyping Systems**
  - Selective Laser Sintering
  - Three-Dimensional Printing

1.3.1 STEREOLITHOGRAPHY

Stereolithography is the most widely used rapid prototyping technology. Stereolithography builds plastic parts or objects a layer at a time by tracing a laser beam on the surface of a vat of liquid photopolymer. This class of materials originally developed for the printing and packaging industries, quickly solidifies wherever the laser beam strikes the surface of the liquid. Once one layer is completely traced, it's lowered a small distance into the vat and a second layer is traced right on top of the first. The self adhesive property of the material causes the layers to bond to one another and eventually form a complete, three-dimensional object after many such layers are formed.

Some objects have overhangs or undercuts which must be supported during the fabrication process by support structures. These are either manually or automatically designed or fabricated right along with the object. Upon completion of the fabrication process, the object is elevated from the vat and the supports are cut off.

Stereolithography generally is considered to provide the greatest accuracy and best surface finish of any rapid prototyping technology. Over the years, a wide range of materials with properties mimicking those of several engineering thermoplastics have been developed. Limited selectively, color changing materials for biomedical and other

applications are available, and ceramic materials are currently being developed. The technology is also notable for the large object sizes that are possible.

On the negative side, working with liquid materials can be messy and parts often require a post-curing operation in a separate oven-like apparatus for complete cure and stability. Recently, inkjet technology has been extended to operation with photopolymers resulting in systems that have both fast operation and good accuracy.

The implementation shown in **Figure 1.4** is used by 3D Systems and some foreign manufacturers. A moveable table, or elevator (A), initially is placed at a position just below the surface of a vat (B) filled with liquid photopolymer resin (C). This material has the property that when light of the correct color strikes it, it turns from a liquid to a solid. The most common photopolymer materials used require an ultraviolet light, but resins that work with visible light are also utilized. The system is sealed to prevent the escape of fumes from the resin. **[1]**

A laser beam is moved over the surface of the liquid photopolymer to trace the geometry of the cross-section of the object. This causes the liquid to harden in areas where the laser strikes. The laser beam is moved in the X-Y directions by a scanner system (D). These are fast and highly controllable motors which drive mirrors and are guided by information from the CAD data.

The exact pattern that the laser traces is a combination of the information contained in the CAD system that describes the geometry of the object, and information from the rapid prototyping application software that optimizes the faithfulness of the fabricated object. Of course, application software for every method of rapid prototyping modifies the CAD data in one way or another to provide for operation of the machinery and to compensate for shortcomings. After the layer is completely traced and for the most part hardened by the laser beam, the table is lowered into the vat a distance equal to the thickness of a layer. The resin is generally quite viscous, however. To speed this process of recoating, early stereolithography systems drew a knife edge (E) over the surface to smooth it. More recently pump-driven recoating systems have been utilized.

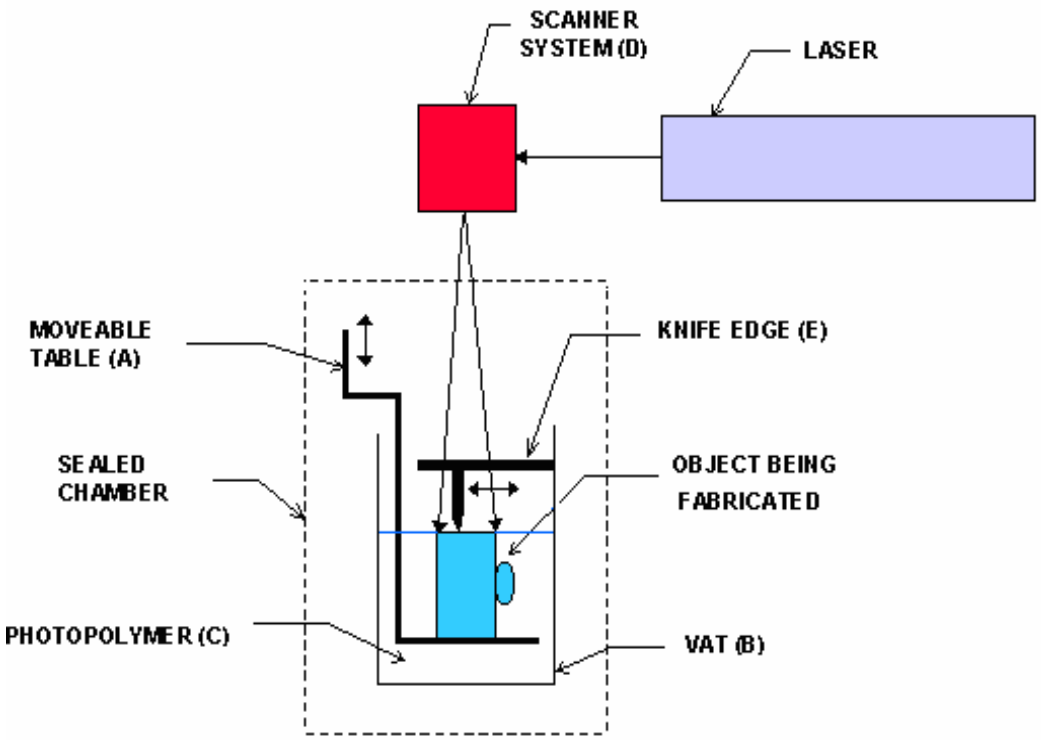

Figure 1.4 Stereolithography

The tracing and recoating steps are repeated until the object is completely fabricated and sits on the table within the vat. Some geometries of objects have overhangs or undercuts. These must be supported during the fabrication process. The support structures are either manually or automatically designed.

Upon completion of the fabrication process, the object is elevated from the vat and allowed to drain. Excess resin is swabbed manually from the surfaces. The object is often given a final cure by bathing it in intense light in a box resembling an oven called a Post-Curing Apparatus (PCA). Some resins and types of stereolithography equipment don't require this operation, however.

After final cure, supports are cut off the object and surfaces are sanded or otherwise finished. Work continues to provide materials that have wider and more directly useable mechanical properties.

1.3.2 SOLID GROUND CURING

In solid ground curing instead of using a laser to expose and harden photopolymer element by element within a layer as is done in stereolithography, a mask is used to expose the entire object layer at once with a burst of intense UV light as shown in **Figure 1.5**. The method of generating the masks is based on electro photography (xerography).

This is a two cycle process having a mask generation cycle and a layer fabrication cycle. It takes about 2 minutes to complete all operations to make a layer. The different operations are:

1. First the object under construction (A) is given a coating of photopolymer resin as it passes the resin applicator station (B) on its way to the exposure cell (C).

2. A mask is generated by electro statically transferring toner in the required object cross sectional image pattern to a glass plate (D) An electron gun writes a charge pattern on the plate which is developed with toner. The glass plate then moves to the exposure cell where it is positioned above the object under construction.

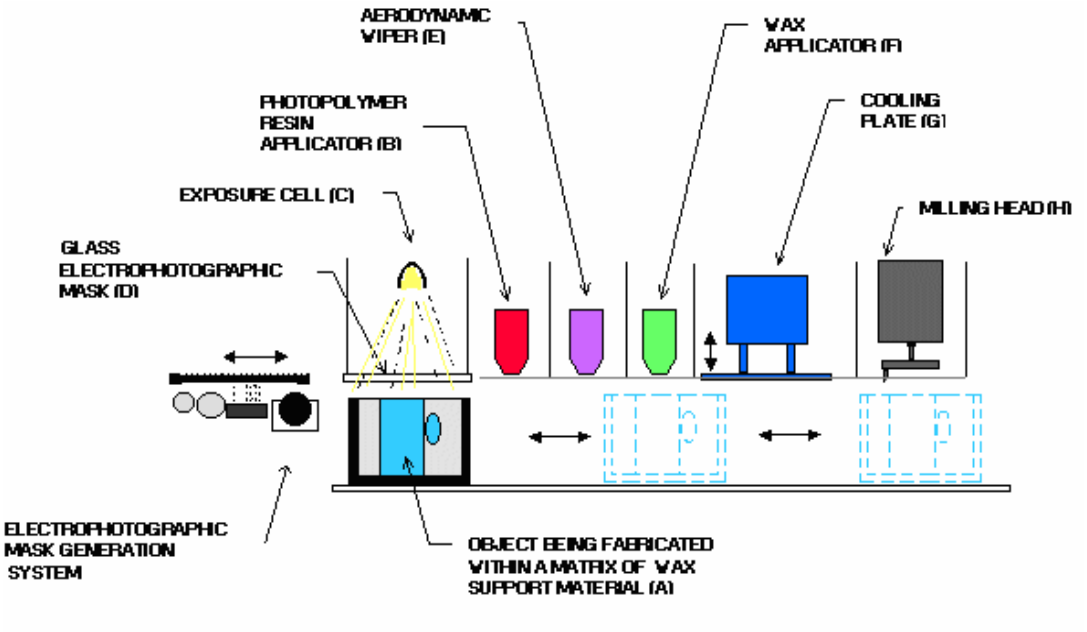

Figure 1.5 Solid Ground Curing

3. A shutter is opened allowing the exposure light to pass through the mask and quickly cure the photopolymer layer in the required pattern. Because the light is so intense the layer is fully cured and no secondary curing operation is necessary as is the case with stereolithography.

4. The mask and object under fabrication then part company. The glass mask is cleaned of toner and discharged. A new mask is electro photographically generated on the plate to repeat the cycle.

5. The object moves to the aerodynamic wiper (E) where any resin that wasn't hardened is vacuumed off and discarded.

6. It then passes under a wax applicator (F) where the voids created by the removal of the unhardened resin are filled with wax. The wax is hardened by moving the object to the cooling station (G) where a cold plate is pressed against it.

7. The final step involves running the object under the milling head (H). Both the wax and photopolymer are milled to a uniform thickness and the cycle is repeated until the object is completely formed within a wax matrix.

Secondary operations are required to remove the wax. It can either be melted away or dissolved using a dish-washing-like machine. The object is then sanded or otherwise finished as is done in stereolithography. The wax matrix makes it unnecessary to generate extra support structures for overhangs or undercuts.

1.3.3 LAMINATED OBJECT MANUFACTURING

In laminated object manufacturing profiles of object cross sections are cut from paper or other web material using a laser. The paper is unwound from a feed roll onto the stack and first bonded to the previous layer using a heated roller which melts a plastic coating on the bottom side of the paper. The profiles are then traced by an optics system that is mounted to an X-Y stage.

In general, the finish, accuracy and stability of paper objects are not as good as for materials used with other RP methods. However, material costs are very low, and objects

have the look and feel of wood and can be worked and finished in the same manner. This has fostered applications such as patterns for sand castings. While there are limitations on materials, work has been done with plastics, composites, ceramics and metals. Some of these materials are available on a limited commercial basis.

Profiles of object cross sections are cut from paper using a CO2 laser as shown in **Figure 1.6.** The paper is unwound from a feed roll (A) onto the stack and bonded to the previous layer using a heated roller (B). The roller melts a plastic coating on the bottom side of the paper to create the bond. The profiles are traced by an optics system that is mounted to an X-Y stage (C). The process generates considerable smoke. Either a chimney or a charcoal filtration system is required (E) and the build chamber must be sealed. After cutting the geometric features of a layer is completed, the excess paper is cut away to separate the layer from the web. The extra paper of the web is wound on a take-up roll (D). The method is self-supporting for overhangs and undercuts. Areas of cross sections which are to be removed in the final object are heavily cross-hatched with the laser to facilitate removal. It can be time consuming to remove extra material for some geometry.

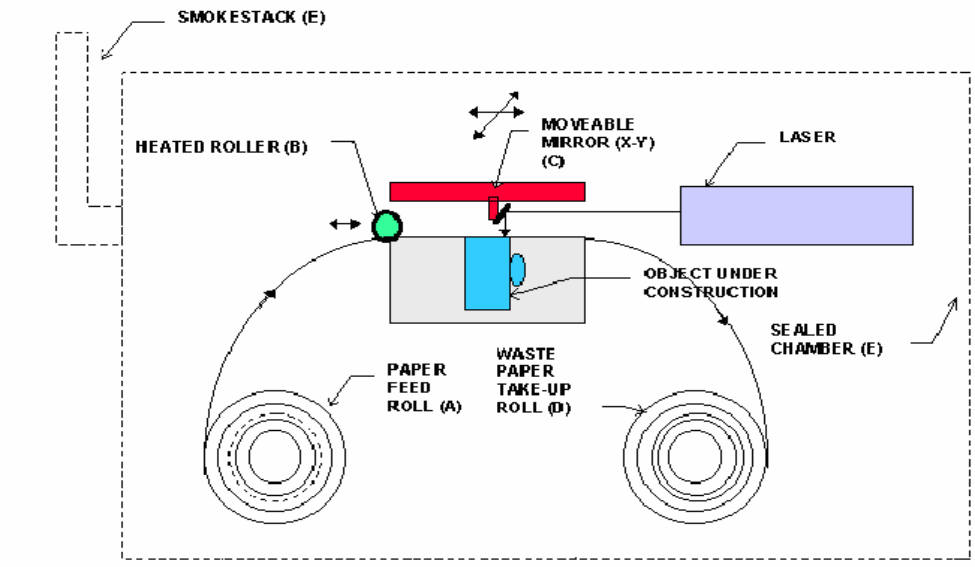

Figure 1.6 Detailed Laminated Object Manufacturing

The finish and accuracy are not as good as with some methods; however objects have the look and feel of wood and can be worked and finished in the same manner.

1.3.4 FUSED DEPOSITION MODELING

FDM is the second most widely used rapid prototyping technology, after stereolithography**.** A plastic filament, approximately 1/16 inch in diameter, is unwound from a coil (A) and supplies material to an extrusion nozzle (B) as shown in **Figure 1.7**. Some configurations of the machinery have used plastic pellets fed from a hopper rather than a filament. The nozzle is heated to melt the plastic and has a mechanism which allows the flow of the melted plastic to be controlled. The nozzle is mounted to a mechanical stage (C) which can be moved in horizontal and vertical directions.

As the nozzle is moved over the table (D) in the required geometry, it deposits a thin bead of extruded plastic to form each layer. The plastic hardens immediately after being squirted from the nozzle and bonds to the layer below. The entire system is contained within an oven chamber which is held at a temperature just below the melting point of the plastic. Thus, only a small amount of additional thermal energy needs to be supplied by the extrusion nozzle to cause the plastic to melt. This provides much better control of the process.

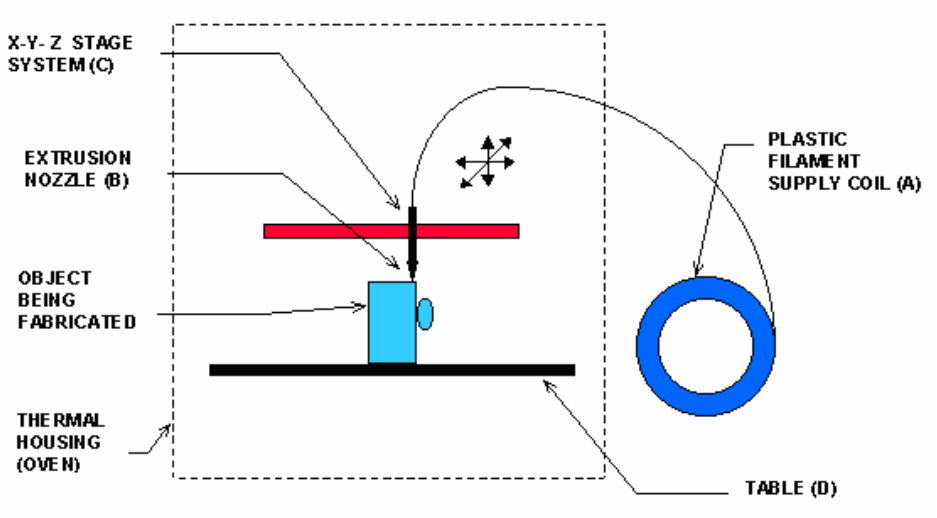

Figure 1.7 Fused Deposition Modeling

Support structures must be designed and fabricated for any overhanging geometries and are later removed in secondary operations. Several materials are available for the process including a nylon-like polymer and both machinable and investment casting waxes. The introduction of ABS plastic material led to much greater commercial acceptance of the method. It provided better layer to layer bonding than previous materials and consequently much more robust fabricated objects.

Also a companion support material was introduced at that time which was easily removable by simply breaking it away from the object. Water-soluble support materials have also become available which can be removed simply by washing them away. The recent introduction of polycarbonate and poly (phenyl) sulfone modeling materials have further extended the capabilities of the method in terms of strength and temperature range. Several other polymer systems as well as ceramic and metallic materials are under development.

The method is office-friendly and quiet. FDM is fairly fast for small parts on the order of a few cubic inches, or those that have tall, thin form-factors. It can be very slow for parts with wide cross sections, however. The finish of parts produced with the method have been greatly improved over the years, but aren't quite on a par with stereolithography. The closest competitor to the FDM process is probably three dimensional printing. However, FDM offers greater strength and a wider range of materials than at least the implementations of 3DP from Z Corp. which is most closely comparable.

1.3.5 SELECTIVE LASER SINTERING

In SLS thermoplastic powder is spread by a roller over the surface of a build cylinder. The piston in the cylinder moves down one object layer thickness to accommodate the new layer of powder. The powder delivery system is similar in function to the build cylinder. Here, a piston moves upward incrementally to supply a measured quantity of powder for each layer. A laser beam is then traced over the surface of this tightly compacted powder to selectively melt and bond it to form a layer of the object. The process is repeated until the entire object is fabricated.

SLS offers the key advantage of making functional parts in essentially final materials. However, the system is mechanically more complex than stereolithography and most other technologies. A variety of thermoplastic materials such as nylon, glass filled nylon, and polystyrene are available. Surface finishes and accuracy are not quite as good as with stereolithography, but material properties can be quite close to those of the intrinsic materials. The method has also been extended to provide direct fabrication of metal and ceramic objects and tools.

Since the objects are sintered they are porous. It may be necessary to infiltrate the part, especially metals, with another material to improve mechanical characteristics. The process is somewhat similar to stereolithography in principle as can be seen in **Figure 1.8.** In this case, however, a laser beam is traced over the surface of a tightly compacted powder made of thermoplastic material (A). The powder is spread by a roller (B) over the surface of a build cylinder (C). A piston (D) moves down one object layer thickness to accommodate the layer of powder. The powder supply system (E) is similar in function to the build cylinder. It also comprises a cylinder and piston. In this case the piston moves upward incrementally to supply powder for the process.

Heat from the laser melts the powder where it strikes under guidance of the scanner system (F). The CO2 laser used provides a concentrated infrared heating beam. The entire fabrication chamber is sealed and maintained at a temperature just below the melting point of the plastic powder. Thus, heat from the laser need only elevate the temperature slightly to cause sintering, greatly speeding the process. A nitrogen atmosphere is also maintained in the fabrication chamber which prevents the possibility of explosion in the handling of large quantities of powder.

After the object is fully formed, the piston is raised to elevate the object. Excess powder is simply brushed away and final manual finishing may be carried out. That's not the complete story, though. It may take a considerable time before the part cools down enough to be removed from the machine. Large parts with thin sections may require as much as two days of cooling time.

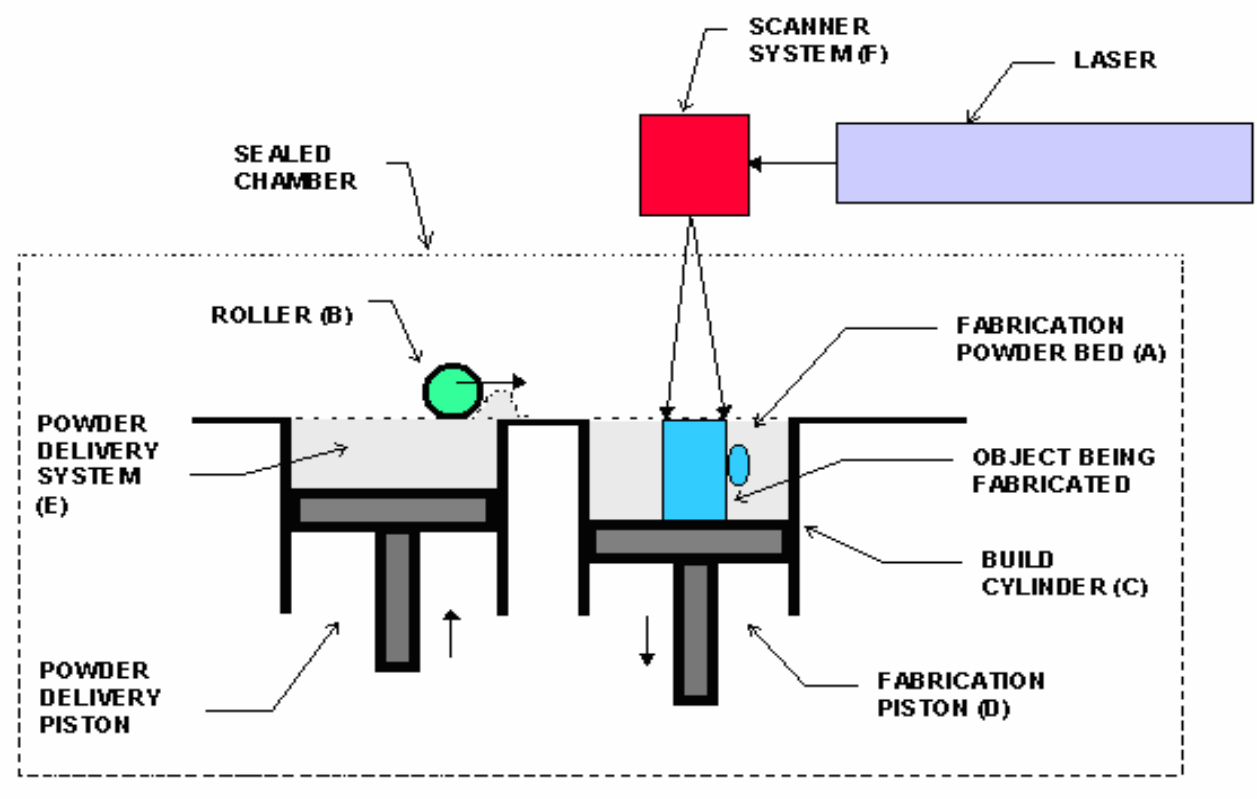

Figure 1.8 Selective Laser Sintering

No supports are required with this method since overhangs and undercuts are supported by the solid powder bed. This saves some finishing time compared to stereolithography. However, surface finishes are not as good and this may increase the time. No final curing is required as in stereolithography, but since the objects are sintered they are porous. Depending on the application, it may be necessary to infiltrate the object with another material to improve mechanical characteristics. Much progress has been made over the years in improving surface finish and porosity. The method has also been extended to provide direct fabrication of metal and ceramic objects and tools.

1.3.6 THREE-DIMENSIONAL PRINTING

The process of three dimensional printing is very reminiscent of selective laser sintering, except that the laser is replaced by an inkjet head. The process starts by depositing a layer of powder object material at the top of a fabrication chamber. The system was developed at MIT and is shown schematically **Figure 1.9**. The multi-channel

jetting head (A) deposits a liquid adhesive compound onto the top layer of a bed of powder object material (B). The particles of the powder become bonded in the areas where the adhesive is deposited. Once a layer is completed the piston (C) moves down by the thickness of a layer.

As in selective laser sintering, the powder supply system (E) is similar in function to the build cylinder In this case the piston moves upward incrementally to supply powder for the process and the roller (D) spreads and compresses the powder on the top of the build cylinder. The process is repeated until the entire object is completed within the powder bed. After completion the object is elevated and the extra powder brushed away leaving a "green" object. Parts must usually be infiltrated with a hardener before they can be handled without much risk of damage.

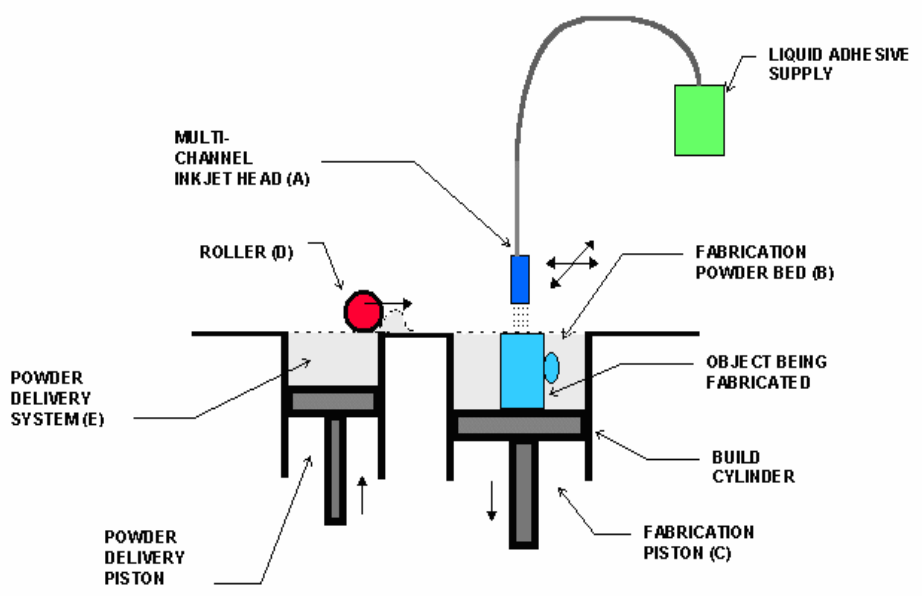

Figure 1.9 Detailed Three Dimensional Printing

No external supports are required during fabrication since the powder bed supports overhangs. Three dimensional printing offers the advantages of speedy fabrication and low materials cost. In fact, it's probably the fastest of all RP methods. Color output is also available; however there are limitations on resolution, surface finish,

part fragility and available materials. The closest competitor to this process in terms of costs and applications is probably fused deposition modeling.

1.4 Comparison of Rapid Prototyping Technologies

Technology	**Sterolithography**	**Laminated object manufacturing**	**Fused deposition modeling**	**Selective laser sintering**	**3-D printing**
Acronym	SLA	LOM	FDM	SLS	3DP
Representati -ve Vendor	3D Systems	Solidimension [sold in US by 3D Systems]	Stratasys	EOS GmbH	Z Corp.
Maximum Build Chamber (inches	20 x 20 x 24	6.29 x 8.26 x 5.31	24 x 20 x 24	27.5 x 15 x 23	20 x 24 x 16
Speed	average	good	poor	average to good	excellent
Accuracy	very good	fair	fair	good	fair
Surface Finish	very good	fair	fair	good to very good	fair
Strengths	large part size, accuracy	price, size	price, materials	accuracy, materials,	speed, price, color
Weaknesses	post processing, messy liquids	limited materials, finish and accuracy	speed	size & wt, system price, surface, finish	Limited, materials, fragile parts, finish

Typical Application	1.Very detailed parts & models for fit & form testing 2.Trade show and marketing parts & models 3.RM of small detailed parts 4.Fabrication of specialized manufacturing tools 5.Patterns for investment casting 6.Patterns for urethane & RTV molding	1.Somewhat less detailed parts & models for fit & form testing compared to other methods 2.Patterns for urethane & RTV molding 3.Larger patterns for sand-casting	1. Detailed parts and models for fit & form testing using engg. plastics 2.Detailed parts for patient- and food-contacting applications 3.Plastic parts for higher-temperature applications 4.Trade show and marketing parts & models 5.Rapid manufacturing of small detailed parts 6.Patterns for investment casting 7.Fabration of specialized manufacturing	1.Slightly less detailed parts and models for fit & form testing compared to photopolymer-based methods using engineering plastics 2.Rapid manufacturing of parts, including larger items such as-air ducts 3.Parts with snap-fits & living hinges 4.Parts	1.Concept models 2.Parts for limited functional testing 3.Color models for FEA and other engineering related applications 4.Architectural & landscape models 5.Color industrial design models, especially consumer goods 6.Castings

			tools	which are durable & provide casting	
System Price Range	$75K-800K	$15K-240K	$19K-300K	$200K-1M+	$20K-70K
Available properties and characteristcs include	1.Acrylics (fair selection) 2.Clear & rigid 3.ABS-like 4.Polypropylene-like (PP) 5.Flexible or elastomeric	1.Bonded PVC-based plastic film 2.Bonded paper	1.ABS 2.Polycarbonate (PC) 3.Polyphenylsulfone 4.Elastomer	1.Nylon, including flame-retardant, glass, aluminum, carbon-filled and others providing increased strength and other properties 2.Polystyrene, Elastomer-ic, Steel and S.S alloys, Bronze alloy, Cobalt-chrome alloy, Titanium	1.Bonded plaster, plaster composite 2.Elastomeric 3.Investment & direct casting
Plastic	$75-110	$18	$115-185	$25-60	
Metal/other		$5-8 (paper)		$35-115/ $5(sand)	Starch $0.35/ cubic inch

CHAPTER-2 LITERATURE REVIEW

2.1 INTRODUCTION

The RP systems can be classified in terms of the material used into photopolymer resin, powder, and wax types. Photopolymer- type RP systems employ lasers to selectively expose the surface of the liquid resin and the absorbance of energy causes photopolymerisation, which converts the liquid resin into a solid. Stereolithography (SL) is one of the most popular commercial RP systems in the industrial world. Powder-type RP systems employ high-power lasers to sinter exposed powder to form the required shape. Wax-type RP systems employ a nozzle to inject the melted wax onto the cold substrate. The common principle is that RP systems use the material phase change to build the part layer by layer.

Volume shrinkage of the resin during the photopolymerisation is one of the major causes leading to poor accuracy of the built prototype. The reaction of photopolymerisation is caused by producing free radicals when the laser energy is applied. The free radicals help the linkage of small molecules (monomers) into large molecules (polymers) comprising of several monomer units**.** The process of linking is exothermic and the temperature in curing a tiny volume rises instantly. The cured volume expands with the exothermic reaction and shrinks after lowering the temperature by thermal equilibrium with the liquid photopolymer which is not cured.

The curing and volume shrinkage occur simultaneously. This dynamic photopolymerisation causes non-uniform internal stress which results in curl distortion in the fabrication process. The dynamic photopolymerisation is related to the volume shrinkage rate of the resin and the building parameters such as laser power, laser scan speed, scan pitch and laser scanning styles. As a result, modeling the stereolithography process is a complicated task. In order to investigate how the built parameters affect the curl distortion and shrinkage, a series of experimental and numerical analyses has been carried out.

2.2 TECHNOLOGY USERS

The following papers show the work done by various researchers in the field of problems dealing with stereolithography type rapid prototyping system.

G. Bugeda *et. al.* [2] developed the finite element formulation for the equilibrium problem involved in SLA processes. The problem involved the solution of a standard set of second-order linear elliptic equations in terms of the displacements u with appropriate boundary conditions:

$$Lu = S^T DSu = v.in.\Omega \quad \textbf{(2.1)}$$

where u is the displacement vector at each point, v is the volumetric force, L is the second- order equilibrium differential operator, S is a first-order operator that provides the strains ε in terms of the displacements $(\varepsilon = Su)$, and D is a matrix containing the elastic constants of the material.

It was assumed that the structural behavior of SLA resins can be modeled using a linear elastic model with constant Young modulus and Poisson ratio. This was an approximation because the resin behavior during the SLA process is inelastic and the material properties do not remain constant.

Discretization of equation (2.1) using standard trial functions N for the approximation of the displacements $(u \approx \sum Na)$ leads to the standard linear system of equations:

$$K\ a\ =\ f_\varepsilon \quad \textbf{(2.2)}$$

with

$$K = \sum_{(e)} K^{(e)} \quad \textbf{(2.3)}$$

$$K^{(e)} = \int_\Omega (e) B^T D B d\Omega \quad \textbf{(2.4)}$$

$$f_\varepsilon\ =\ \sum_{(e)} f_\varepsilon^{(e)} \quad \textbf{(2.5)}$$

$$f_\varepsilon^{(e)}\ =\ \int_\Omega (e) B^T D\ \varepsilon^0 d\Omega \quad \textbf{(2.6)}$$

where K, a and f_ε denote the stiffness matrix, the nodal displacements and the equivalent nodal force vector caused by volumetric strains. Only gravity body forces were neglected in the analysis. Matrix $B = SN$ was used to obtain the strains at each point in terms of the nodal displacements as $\varepsilon = Ba$, and the constitutive matrix D relates strains to stresses as $\sigma = D\varepsilon$. The superscript $^{(e)}$ relates to a single finite element. The vector ε^0 contains the volumetric shrinkage of the resin:

$$\varepsilon^0 = \left[\varepsilon^0, \varepsilon^0, 0\right]^T \text{ (For two-dimensional problems);} \quad \textbf{(2.7)}$$

$$\varepsilon^0 = \left[\varepsilon^0, \varepsilon^0, \varepsilon^0, 0, 0, 0\right]^T \text{ (For three-dimensional problems)} \quad \textbf{(2.8)}$$

Linear and quadratic elements were used for the solution of equation (2.1). Linear elements didn't produce good solutions when parts were subjected to bending deformation. On the other hand, the use of quadratic elements was much more expensive than that of linear elements. In order to improve the behavior of linear elements, a selective integration scheme was used. This technique involved the sub integration of the part of the stiffness matrix that corresponds to shear terms. For each element (e) its stiffness matrix $K^{(e)}$ was decomposed in two parts. The first one $K_v^{(e)}$ contains the volumetric terms, and the second one, $K_t^{(e)}$ contains the shear terms:

$$K^{(e)} = K_v^{(e)} + K_t^{(e)} \quad \textbf{(2.9)}$$

with

$$K_{v_{i,j}}^{(e)} = \int^{\Omega(e)} B_{v_i}^T D_v B_{v_j} d\Omega \quad \textbf{(2.10)}$$

$$K_{t_{i,j}}^{(e)} = \int^{\Omega(e)} B_{t_i}^T D_t B_{t_j} d\Omega \quad \textbf{(2.11)}$$

For the two-dimensional case, these expressions were particularized to:

$$B_{v_i} = \begin{bmatrix} \frac{\partial N_i}{\partial x} & 0 \\ 0 & \frac{\partial N_i}{\partial y} \end{bmatrix} \quad \textbf{(2.12)}$$

$$B_{t_i} = \begin{bmatrix} \frac{\partial N_i}{\partial x} & \frac{\partial N_i}{\partial y} \end{bmatrix} \quad \textbf{(2.13)}$$

and $$D_v = \begin{bmatrix} d_{11} & d_{12} \\ d_{21} & d_{22} \end{bmatrix}; \; D_t = \begin{bmatrix} d_{33} \end{bmatrix} \quad \textbf{(2.14)}$$

and for the plane stresses case:

$$d_{11} = d_{22} = \frac{E}{1-\nu^2} \quad \textbf{(2.15)}$$

$$d_{12} = d_{21} = \nu d_{11} \quad \textbf{(2.16)}$$

$$d_{33} = \frac{E}{2(1+\nu)} = G \quad \textbf{(2.17)}$$

where E and ν are Young's modulus and Poisson's ratio respectively. Matrix K_v was computed using a second order integration scheme whereas matrix K_t was computed using a first-order integration scheme.

R.S.Chambers *et. al.* [3] used finite element method to develop the framework for a tool that can be used to model the structural deformations arising from sterolithography build process. Although the software at that time made an attempt to capture all the physics of the process, provisions for three important build features were made: 1) laser path history including scanning rate and depth cure, 2) structural linkage, and 3) time varying material behavior. For demonstration purposes, a three dimensional finite element code was modified to include a phenomenological material model of solidification. The model was based on cure shrinkage and stress relaxation data was collected by in-situ tests on individual strands drawn using 3D Systems Sterolithography apparatus (SLA-250). To depict the directed path of solidification within layers, a finite element birthing scheme was conceived to activate elements along the predetermined coordinate path of laser. Structural linkage was enforced by joining strands or layers when laser paths connect or overlap, respectively. A limited number of analyses were performed to contrast build styles.

B. Wiedemann *et. al.* [4] developed methods which evaluate photopolymers with respect to dynamics of polymerization and shrinkage, and also the sensitivity of polymerization with respect to process conditions and ambient influences, to facilitate the selection of stereolithography resins. It was also discussed that how numerical simulation of part distortion can help in understanding the interaction between material properties and process parameters. Finally it was concluded that the building process must be optimized to reduce internal stresses and to cater post-curing effects.

T.R.Guess *et. al.* [5] studied how to generate material properties that can be used to develop phenomenological material models of epoxy and acrylate resins. Strands tests were performed in situ in a 3D System's SLA -250 machine; strands were drawn by either single or multiple exposures of the resin to a laser beam. Linear shrinkage, cross-sectional areas, cure shrinkage forces and stress-strain data were presented. Also, the curl in cantilever beam specimens, build with different draw patterns, were compared.

H. Narahara *et. al*. [6] studied the relation between the scanned laser beam and initial linear shrinkage in a very small volume. In order to discuss the curing behavior of the resin in a minute volume, discussion of only the shrinkage behavior of a single strand was not sufficient. The measured output, which corresponds to the linear shrinkage, did not agree with the minute volume behavior, as a single strand consists of a serial connection of minute volumes while the measurement data contains serial effects. It was necessary to remove the serial effects and extract the minute volume curing behavior from the measured data of a single strand.

Consequently, a mathematical relation of the experiment was formulated. Linear shrinkage $\varepsilon_s(t)$ and $\varepsilon_p(t)$ was defined as follows:

$\varepsilon_s(t)$ **:** The time history of the average linear shrinkage of a single strand produced by the laser irradiation which connects fixed ends and free ends.

$\varepsilon_p(t)$ **:** The time history of the linear shrinkage of cured resin with minute length divided by the scanning direction after laser irradiation.

The length ℓ of a single strand was drawn from a fixed end to a free end by laser scanning as shown in **Figure 2.1**:

The time history of the linear shrinkage $\varepsilon_s(t)$ was measured by the sensor. The time when the laser beam reaches the free end was defined as 0**.** The time history of the minute volume linear shrinkage was defined as $\varepsilon_p(t)$.

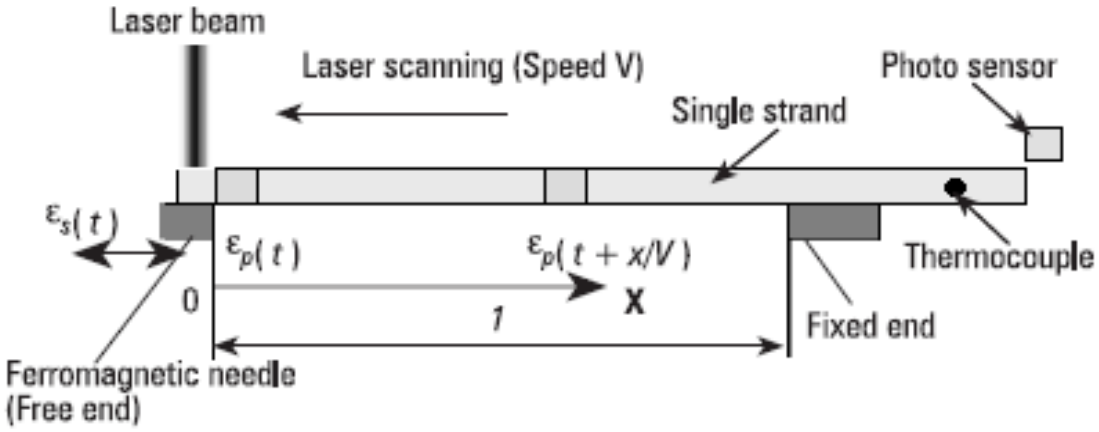

Figure 2.1 Definition of measured linear shrinkage and minute volume linear shrinkage

Considering that the laser beam scans at speed V**,** the minute volume linear shrinkage $\varepsilon_p(t)$ should have the same characteristics at every part of the single strand except different starting times. Therefore, the time history of the measured linear shrinkage $\varepsilon_s(t)$ is equal to the integration of the $\varepsilon_p(t)$ with a time delay that corresponds to the scanning speed V**:**

$$\varepsilon_s(t) = \frac{1}{\ell}\int_0^{\ell} \varepsilon_p\left(t + \frac{x}{V}\right)dx = \frac{V}{\ell}\int_t^{t+\frac{\ell}{V}} \varepsilon_p(u)\,du \qquad \textbf{(2.18)}$$

By differentiating the integral relation, the minute volume linear shrinkage $\varepsilon_p(t)$ was derived from the following equation:

$$\varepsilon_p = -\frac{1}{V}\frac{\partial \varepsilon_s(t)}{\partial t} + \varepsilon_p\left(t + \frac{\ell}{V}\right) \qquad \textbf{(2.19)}$$

Since this equation had the term $\varepsilon_p(t)$ on the right side, $\varepsilon_p(t)$ can't be solved by equation (2) only. An additional relation was required. After sufficient passing time, the linear shrinkage becomes uniform in the length direction. Thus, the value of the linear shrinkage of a single strand becomes identical to the linear shrinkage of a minute volume:

$$\varepsilon_s(\infty) = \varepsilon_p(\infty) \tag{2.20}$$

Therefore $\varepsilon_p(t)$ was obtained by the backward substitution of strain $\varepsilon_s(t)$, which was a backward time history of measured linear shrinkage from the initial exposure up to the steady state. It means that the $\varepsilon_p(t)$ value was obtained from the time infinity, or steady state, to zero from this equation. Using the sampled data $\varepsilon_s(t)$ from time t = 0 to t_a , $\varepsilon_p(t)$ was solved as equation (5), where Δt is the sampling time, t_a is the final measuring time and M is the total sampling number. For obtaining better resolution and calculation results, the relation $0 < (\Delta t << \ell / V << t_a)$ must be satisfied:

$$t_a = M.\Delta t, \frac{\ell}{v} = K.\Delta t, \tag{2.21}$$

$$t = N.\Delta t \left(N = 0,1,2,.....M\right) \tag{2.22}$$

$$\varepsilon_p\left(t_a - \frac{\ell}{V}\right) = -\frac{\ell}{V}\frac{\partial \varepsilon_s\left(t_a - \frac{\ell}{V}\right)}{\partial t} + \varepsilon_s(t_a) \tag{2.23}$$

$$\varepsilon_p\left((M-K).\Delta t\right) = -\frac{\ell}{V}\frac{\partial \varepsilon_s\left((M-K).\Delta t\right)}{\partial t} + \varepsilon_s(M.\Delta t) \tag{2.24}$$

$$\vdots$$

$$\vdots$$

$$\varepsilon_p = \left((M-2K+1)\Delta t\right) = -\frac{\ell}{V}\frac{\partial \varepsilon_s\left((M-2K+1)\Delta t\right)}{\partial t} + \varepsilon_s\left((M-K+1).\Delta t\right) \tag{2.25}$$

$$\varepsilon_p\left((M-2K).\Delta t\right) = \frac{\ell}{V}\frac{\partial \varepsilon_s\left((M-2K).\Delta t\right)}{\partial t} + \varepsilon_p\left((M-K).\Delta t\right) \tag{2.26}$$

$$\vdots$$

$$\varepsilon_p(\Delta t) = -\frac{\ell}{V}\frac{\partial \varepsilon_s(\Delta t)}{\partial t} + \varepsilon_p\left((K+1).\Delta t\right) \tag{2.27}$$

$$\varepsilon_p(0) = -\frac{\ell}{V}\frac{\partial \varepsilon_s(0)}{\partial t} + \varepsilon_p(K.\Delta t) \qquad \textbf{(2.28)}$$

Thus, the time history of minute volume linear shrinkage $\varepsilon_p(t)$ was obtained from the measured data. It was noted that the differential value of $\varepsilon_s(t)$ should be calculated using the smoothed $\varepsilon_s(t)$ that was not affected by the measuring noise.

H.S. Cho *et. al.* [7] focused on increasing build accuracy by optimally designing the process parameters. The process was modeled and described by a multilayer perceptron neural network. Based on that modeled process, the genetic algorithm searched the optimal process parameters so that optimal conditions yield minimum part build error. In practice, genetic algorithms find near-optimal conditions since they do not guarantee true optimal condition. The nearly optimized process was validated by actually building H-parts and comparing these results with those obtained by the currently used nominal condition.

W. L. Yao *et. al.* [8] presented a finite element analysis (FEA) based numerical simulation of the thermal stresses generated during the pattern burnout process. For efficient numerical simulation, an equivalent force technique was developed for the FEA. The predicted thermal stresses agree fairly well with the measured stresses by strain gauges mounted on the test samples of webbed epoxy patterns. Using the finite element analysis, three internal web structures of stereolithography patterns are compared. The FEA results show that the maximum thermal stress with the hexagonal web structure was 22% less than that with the square web structure and 32% less than that with the triangular web structure. The FEA results were useful to the development of computer aided engineering tools for the design of the pattern's internal web structure.

S H Lee *et. al.* [9] investigated that the build method still limits wider applications due to the unsatisfactory level of dimensional accuracy that remains with the current technology. To improve accuracy and reduce part distortion, understanding the physics involved in the relationship between the operating input parameters and the part dimensional

accuracy is prerequisite. In this paper, this causality was identifed through a process model obtained via an artifcial neural network based upon 140 actual build parts. The network was so constructed that it relates the process input parameters to part dimensional accuracy. The neural network model was found to predict the effects of the input parameters on the accuracy with reasonable accuracy. The predicted performance was discussed in detail for various process parameter ranges.

S. S. Hur *et .al.* [10] realized that thermal deformation and residual stresses generated in the stereolithography product must be understood in order to employ the three-dimensional stereolithography for high-precision model building. The purpose of their study was to understand how residual stresses are generated in the three-dimensional stereolithography by solving the governing equations for heat transfer and nonlinear polymerization reaction kinetics simultaneously with finite-difference/finite-element numerical methods. Two cases were considered for the basic understanding of stereolithography. One was when the laser beam stays at one point and the other was when the laser scans along one line. In both cases it was possible to determine the rate of polymerization, heat generation, and the heat-transfer rate in the two-dimensional domain at any time.

As the result of numerical prediction, the distribution of temperature, thermal stress, rate of polymerization, percent conversion, photo-initiator concentration, and laser-light intensity was obtained in the defined domain. In stereolithography, the rate of polymerization and temperature increase rapidly at the initial stage and become stable as time elapses. The photo-initiator concentration decreases as time passes, but it was not influenced significantly by the rapid increase in the rate of polymerization or in temperature. Changes in temperature, heat-transfer rates, and thermal stresses were substantial in the region directly exposed to the laser.

The polymerization reaction, heat transfer, and thermo elasticity were considered at the same time to predict temperature distribution, thermal stress profile, and thermal deformation in the defined analysis domain. Four equations for reaction kinetics were solved by a finite-difference method and one energy equation was solved by a finite-element method. For stationary-laser-beam and moving-laser-beam problems,

percent conversion, rate of polymerization, photo-initiator concentration, temperature profile, residual stress contour, and thermal deformation were obtained.

Theoretical Modeling

It is assumed for the analysis of polymerization reaction kinetics that dark polymerization does not take place. The inhibition effect due to the oxygen dissolved in the monomer resin through the surface is ignored. Optical effects such as scattering, deflection, refraction, and diffraction of the laser light are neglected. It is also assumed that the laser light is absorbed only by the photo-initiator.

A small rectangular domain for modeling of the polymerization reaction is shown in **Figure 2.2**. In the 2-D polymerization domain, the photo-sensitive resin

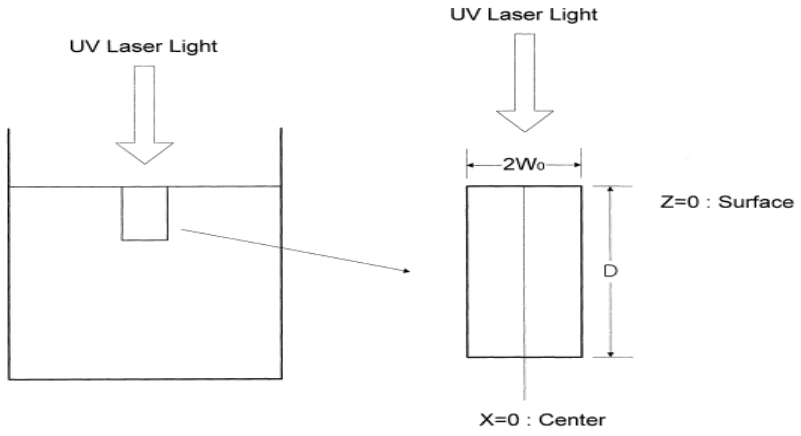

Figure 2.2.Rectangular polymerization domain used for reaction simulation. D =slice depth; W_0 = beam radius.

is solidified by the exothermic chemical reaction. The rate of attenuation in the laser-light intensity with respect to the *z* direction is given by:

$$\frac{\partial I}{\partial z} = -\varepsilon S I \qquad \textbf{(2.29)}$$

$$I(x,y,z) = I_0 \exp\left[-2\left(\frac{x}{W_0}\right)^2\right] \quad \text{at } z = 0 \qquad \textbf{(2.30)}$$

$$I(x,y,z) = I_0 \quad \text{at } x = 0 \qquad \textbf{(2.31)}$$

where I is the laser-light intensity, W_0 is the radius of the laser beam, ε is the molar absorbity of the photo-initiator, and S is the molarity of the photo-initiator. Change in the molarity of the photo-initiator with respect to time is expressed as:

$$\frac{\partial S}{\partial t} = -\phi \varepsilon I \tag{2.32}$$

$$S(x, y, z) = S_0 \qquad \text{at } t = 0 \tag{2.33}$$

where ϕ is the quantum yield. Because the monomer is being consumed as the polymerization reaction proceeds, the rate of decrease in the molarity of the monomer is equivalent to the rate of polymerization:

$$\frac{\partial M}{\partial t} = -R_p \tag{2.34}$$

$$M(x, y, z) = M_0 \qquad \text{at } t = 0 \tag{2.35}$$

where S is the molarity of the monomer and R_p is the rate of polymerization. The rate of photo-initiated polymerization is given by the following equation using the radical chain-reaction kinetics:

$$R_p = k_p M \left(\frac{\phi}{k_t} \varepsilon S I \right)^{0.5} \tag{2.36}$$

Equation (2.35**)** becomes

$$\frac{\partial M}{\partial t} = -k_p M \left(\frac{\phi}{k_t} \varepsilon S I \right)^{0.5} \tag{2.37}$$

where k_p is the kinetic constant of propagation and k_t is the kinetic constant of termination. The degree of polymerization, C, is defined as:

$$C = \frac{M_0 - M}{M_0} \times 100 \tag{2.38}$$

The ratio of k_p to $k_t^{0.5}$ shows an Arrhenius-type behavior and depends on the degree of polymerization:

$$\frac{k_p}{k_t^{0.5}} = k_0 \exp\left[-\frac{E_a}{R}\left(\frac{1}{T}-\frac{1}{T_0}\right)\right] \qquad \textbf{(2.39)}$$

where the constant k_0 and the activation energy E_a are dependent on the degree of polymerization and R is the universal gas constant.

Some assumptions are made for the heat-transfer analysis in the two rectangular domains shown in **Figure 2.3**. When the laser stays at one point, the heat transfer domain shown in **Figure 2.3a** is used for the numerical calculation, and when the laser moves linearly, the heat-transfer domain shown in **Figure2.3b** is used. Heat loss at the surface of the resin in the vat is neglected and the change in material constants due to temperature variation is also neglected. Neglecting heat conduction in the y direction and convection heat transfer in the domain, the energy equation becomes,

$$\rho C_p \frac{\partial T}{\partial t} = k\left(\frac{\partial^2 T}{\partial x^2}+\frac{\partial^2 T}{\partial z^2}\right) + \Delta H_p R_p \qquad \textbf{(2.40)}$$

where is the density, C_p is the specific heat, and k is the thermal conductivity. A finite-difference method is employed to solve the equations for reaction kinetics and a finite-element method is employed to solve the energy equation with proper initial and boundary conditions. A computer program is coded by using C^{++} with the OOP (Object Oriented Programming) technique for further revision and enlargement.

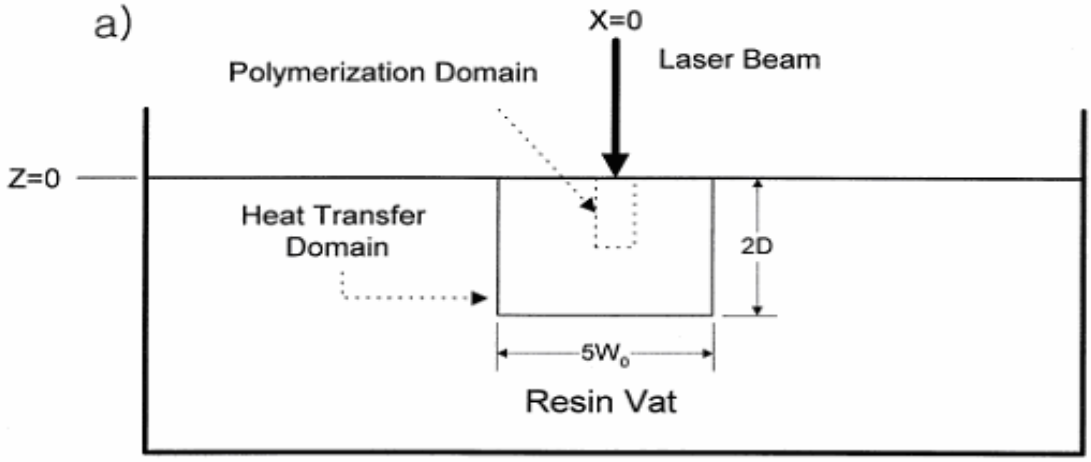

(a)Heat transfer domain used for the one-point problem

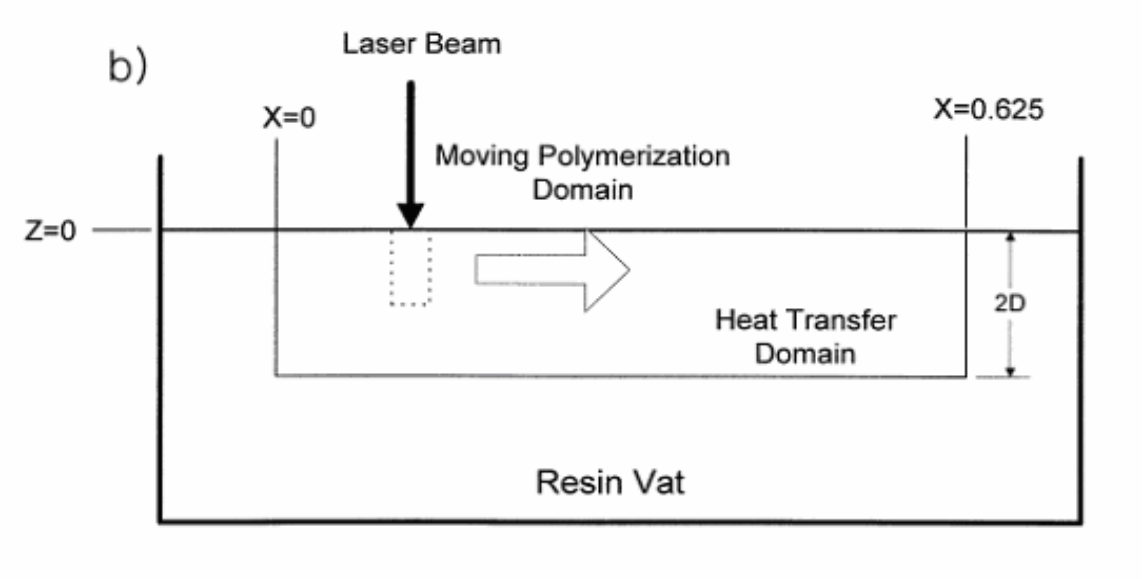

(b)Heat-transfer domain used for the line problem

Figure 2.3 Rectangular heat-transfer domain used for thermal analysis

Y.M. Huang *et al.* [11] presented an innovative rapid prototyping (RP) system using direct mask photo curing (DMPC). The underlying principle of RP system is to fabricate a three-dimensional part layer by layer. The design concept of the DMPC RP system was to use a dynamical photo mask for the layer profile. The image of the dynamic mask, generated by a thin film transistor liquid crystal displayer (TFT LCD) panel, was calculated from the slicing data of the CAD model. In the DMPC system, the photo-polymer is exposed and shielded by the LCD mask, and the light source to cure the photopolymer is from the bottom of the transparent resin container. A residual force is formed between the layer of the cured photo-polymer and the silicon film on the container. This residual force was measured using a load cell and its theoretical model is further developed and simulated using finite element method. Hence, the force measurement, force simulation, layer imagine calculation, LCD control, position control and process parameters were supported by a host computer. As a result, good quality part with low cost can be built by this proposed DMPC RP system.

The usage of silicon film and the control of the over curing depth made it feasible to fabricate a part with better accuracy and surface finish in the DMPC RP system. This low cost and user-friendly interface DMPC RP system was well

suitable for desktop concept model applications. The computer supported force analysis and dynamic control of LCD mask was successfully applied to the DMPC RP system to solve the problem of pulling force and the accuracy sacrifice. A 3D turbine blade benchmark was fabricated by the DMPC and SLP-4000 RP system respectively to evaluate the performance of the DMPC RP system. It demonstrated that the accuracy of the evaluated part has been significantly improved and the cost of the DMPC RP system is much lower than that of all the available commercial RP systems.

D. Karalekas *et. al.* [12] worked on a experimental study to investigate the shrinkage characteristics of acrylic-based and epoxy-based stereolithography (SL) photopolymer resin systems after they have been laser cured and post-cured under ultraviolet (UV), and thermal exposure. The induced residual stresses and strains were determined by the shadow moire and the hole-drilling strain-gage methods. Out-of-plane displacements (warpage) of acrylic-based post-cured resin plates were recorded by means of the shadow moire method and correlated to the shrinkage strains by theoretical analysis. The induced residual stresses in the epoxy-based cylindrical resin specimens were determined from strains of three element strain-gage rosettes of the blind-hole drilling method. Results were presented for the shrinkage stresses and strains for both material systems as a function of the post-curing process (UV, thermal). It was found that the shrinkage strains in the acrylic-based photopolymer resin were of considerable magnitude, while thermal post-curing resulted in higher shrinkage stresses for both material systems. The values of the shrinkage stresses compare well with those of the existing literature.

Y.M. Huang *et. al.* [13] studied that dynamic photopolymerisation is a key issue of an SL rapid prototyping system. The photopolymerisation starts when the absorption of laser energy exceeds a critical quantity. The curing, exothermic reaction, cooling and shrinkage occur in a very short time during the photopolymerisation. The absorption ratio of laser energy affects the curing properties such as cure ratio, elastic modulus and shrinkage behaviour. The absorption ratio of laser energy was controlled by the scan path, scan speed and exposure time. The laser sources illuminate the photopolymer surface from the top. The cure ratio of resin under the current layer increased because of

the re-exposure by the laser penetration, and also because of the shrinkage. Therefore, this was the foundation for developing a dynamic finite element simulation code to investigate curing behaviour in photopolymerisation in the SL rapid prototyping system. So the following conditions during photopolymerisation were considered and the algorithm of the dynamic finite element was presented. The behavior of the cured resin was a function of absorbance laser exposure *E* and elapsed time *t*. The uncured liquid becomes more viscous because of the exothermic temperature of the cured resin. As a result, the deformation of the resin consists of elements as follows:

$$\{\Delta\varepsilon\} = \{\Delta\varepsilon^{e}\} + \{\Delta\varepsilon^{\gamma}\} + \{\Delta\varepsilon^{T}\} + \{\Delta\varepsilon^{v}\} + \{\Delta\varepsilon^{p}\} \qquad \textbf{(2.41)}$$

where $\{\Delta\varepsilon^{e}\}$ indicates the elastic strain, $\{\Delta\varepsilon^{\gamma}\}$ is the strain of cure shrinkage that can be expressed as $\Delta\beta(E,t)$, $\{\Delta\varepsilon^{T}\}$ is the thermal strain that was rewritten as $\alpha\Delta T$, $\{\Delta\varepsilon^{v}\}$ is the viscous strain, and $\{\Delta\varepsilon^{p}\}$ is the plastic strain. During the photopolymerisation process, the plastic strain was relatively small that's why neglected. A case in which $\{\dot{\sigma}\}$ is equal to $[D]\{\dot{\varepsilon}^{(e)}\}$ and $\{\dot{\varepsilon}\}$ is equal to $[B]\{\dot{u}\}$ was considered and by substituting the relationship above and $\int dV[B]^{T}[D]$ into Eq. (1), the following equation was formulated:

$$\int_{v} dV\Big[[B]^{T}[D]\{u\} - [B]^{T}\{\sigma\} - [B]^{T}(3K)\{\alpha\Delta T + \Delta\beta(E)\} = 0\Big] \qquad \textbf{(2.42)}$$

Consequently, the constitution equation of dynamic finite element analysis for the stereolithography process was written as $[K]\{u\} - \{f\} = 0$ **,** and the stiffness matrix was expressed as:

$$[K] = \int_{v} dV\Big[[B]^{T}[D][B]\Big] \qquad \textbf{(2.43)}$$

The effective nodal force was given by:

$$\{f\} = \int_{v} dV\Big[[B]^{T}\{\dot{\sigma}\} + [B]^{T}(3K)\{\alpha\Delta T + \Delta\beta(E)\}\Big] \qquad \textbf{(2.44)}$$

Elastic Modulus and Poisson's Ratio

In the process of photopolymerisation, the increasing of molecular weight and the cross-linking of the monomer cause phase transition in the photopolymer from the liquid state to the solid state. This result leads to the increase of the strength of photopolymer. The phenomenon was explored and the mathematical model of the elastic modulus of curing resin Y was considered to be a function of exposure energy E and exposure time t, which was given as:

$$Y(E,t) = Y_{MAX}\left(1 - e^{-\beta\left(\frac{E}{E_c}-1\right)}\right)\left(1 - e^{-\alpha t}\right)\beta \qquad \textbf{(2.45)}$$

where Y_{MAX} is the maximum elastic modulus, E_c is the critical exposure quantity, α and β were dimensionless constants of which β is directly proportional to E_c.

In order to establish the relationship of the elastic modulus and time, a thermo mechanical analysis (TMA) instrument was used to measure the deformation characteristic of glass transition in the photopolymerisation process. When the temperature rises above the glass transition temperature T_g, the curing resin exhibited a change from a glass-like behavior to a soft and rubber-like behavior. A complete mathematical model of elastic modulus was proposed in order to describe this phenomenon as:

$$Y(E,t) = Y_{MAX}\left(1 - e^{-\beta\left(\frac{E}{E_c}-1\right)}\right)\left(1 - e^{-\alpha t}\right)\gamma \qquad \textbf{(2.46)}$$

where γ is defined as $f(T)/f$ (room temperature) that can be obtained from the relationship of reaction rate and exposure time, and T is the temperature. An important influencing factor during the photopolymerisation was the expansion coefficient. Another was the shrinkage during the thermal equilibrium process. The curing resin part expands because of the exothermic reaction during the photopolymerisation process. The expansion behavior was measured by TMA. The standard measuring sample was a rectangular section of 0.5×0.5 cm^2 and 1 cm thickness. It was fabricated using an 8 mm s^{-1} scanning speed and 0.1 mm scan pitch.

Generally, the penetration depth depends on the laser energy and exposure time. Hence, the concentration decreases layer by layer owing to the disintegration of initiators which causes additional absorption of the exposed energy. Therefore, the effective exposure in the middle of part of the polymer by transmission through the upper layers was given by the following equation 2.47:

$$E_n = E_0 . \exp\left(-z'/D_p\right)\left[1+\exp\left(-d/D_p\right) + \exp\left(-2d/D_p\right)+\ldots+\exp(-(n-1)d/D_p)\right] \quad \textbf{(2.47)}$$

where E_0 is the exposure energy at the surface of the resin, z' is the investigated depth in the layer and D_p is the average penetration depth per layer. Consequently, equation (2.46) was rewritten as:

$$Y\left(E,t\right) = Y_i + \left(Y_F - Y_i\right)\left[1-\exp\left[-\alpha\left(T\right)t\right]\right]\alpha\beta \quad \textbf{(2.48)}$$

$$Y_F = \left(Y_{MAX} - Y_{MIN}\right).\left[1-\exp\left[-\beta\left(\frac{E}{E_c}\right)-1\right]\right].f_y\left(T\right) + Y_{MIN} \quad \textbf{(2.49)}$$

where f_y is the ratio of the elastic modulus coefficient which is a function of temperature and subscript i indicates the number of exposures. The constants Y_{MAX} and Y_{MIN} are the maximum and minimum elastic modulus, respectively. The constants β and α were calculated, respectively, to be 0.44 and 0.31 from the tensile test. In other words, the shrinkage rate a function of the absorption exposure energy and elapsed time and was obtained. A dynamic mathematical model of the cured shrinkage was established as follows:

$$\varepsilon_n = \varepsilon_{final}\left(E_n\right)\left(1-e^{-\alpha_\varepsilon t}\right) \quad \textbf{(2.50)}$$

where ε_n is the total cure shrinkage under exposure E_n and α_ε is a constant. It was derived as:

$$\varepsilon\left(E,t\right) = \varepsilon_{max}\left\{1-\exp\left[-\alpha_a\left(\frac{E}{E_c}\right)-\alpha_b t\right]\right\}\left[1-\exp\left(-\alpha_c t\right)\right] \quad \textbf{(2.51)}$$

where ε_{max} is the maximum cured shrinkage, α_a was the coefficient of the cure reaction rate at the initial laser exposure, α_b was used to model the continuing shrinkage and α_c was used to illustrate the initial part of the cured shrinkage curve. The higher the α_a, the more rapid the reaction occurs in the cure shrinkage.

Rezoning of Uncured Liquid Elements

This was a selective curing process, as like stereolithography. Only the exposed liquid elements were solidified and deformed, but the others kept their original forms. If the shrinkage and curl distortion occur in the exposed liquid element during the current layer scanning, the uncured element may be over distorted. This caused the continuity of global stiffness to be interrupted in the process of simulation. Therefore, it was necessary to reconstruct the elements during the simulation process by using a rezoning technique. The rezoning technique in the development of DFEM program was used to define an addictive new layer mesh on the surface of the curl distortion resin and to transfer the state of the old mesh to the new one. In general, the cured part may be warped out of the next liquid surface layer when the platform was moved down a layer thickness for adding the next layer of resin as shown in **Figure 2.4(*a*).** However, the added liquid elements lie along the surface of cured elements as shown in **Figure 2.4(*b*).**Some of elements located in the boundary between the air and liquid were reconstructed. In the depth direction, these kinds of elements were determined again to keep them parallel with the liquid surface as shown in **Figure 2.4(*c*).**

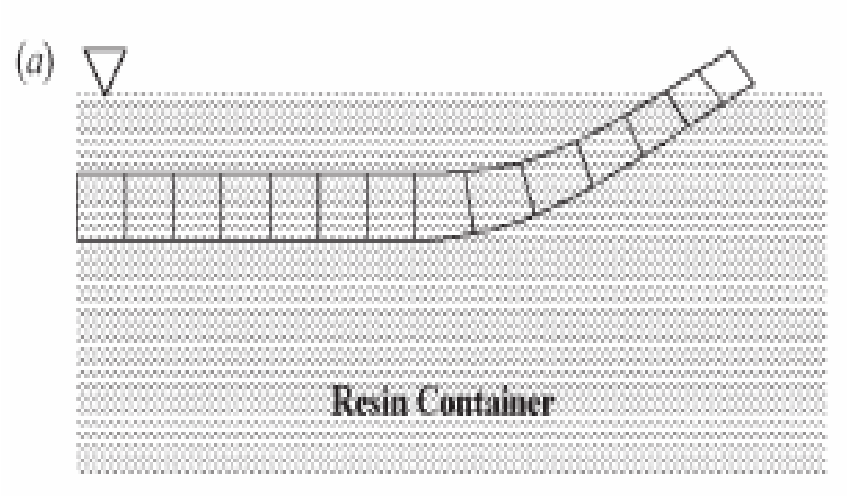

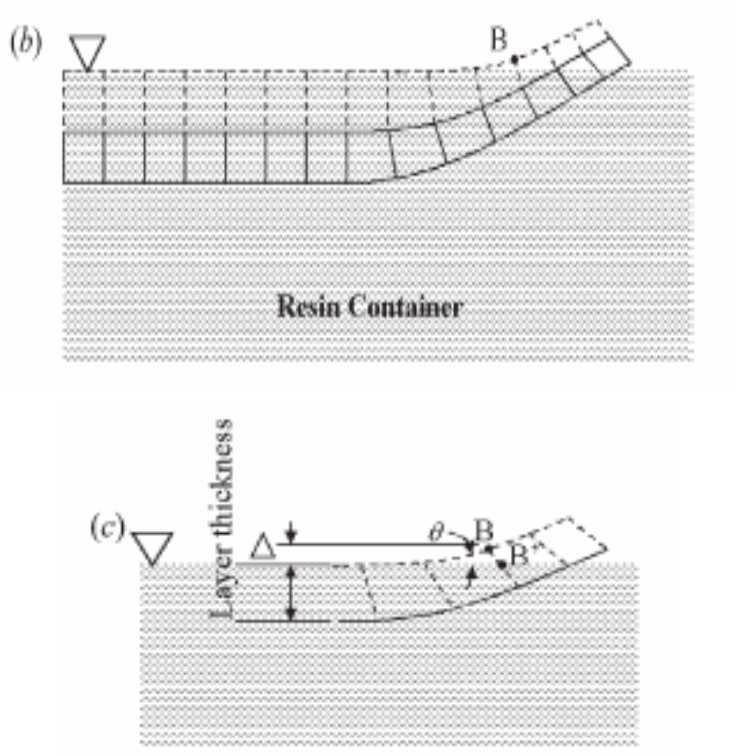

Figure 2.4 Scheme of the rezoning technique

Therefore, the node B was moved to B'. The different distances of the closet node B, which is above the liquid surface, was set as a variable Δ the other nodes were moved slightly along the *x*-axis according to

$$\Delta_{jx} = \delta_x . \Delta . \sec\theta \qquad \textbf{(2.52)}$$

where subscript j is the node number, which is located above the current liquid surface, and δ_x is a rezoning factor in the range 0.1 to 0.01 corresponding to the size of the used element. The smaller the element size used, the smaller the rezoning factor employed.

Development of Dynamic Finite Element Method

According to the theoretical model, the development of DFEM was based on the dynamic material behaviour. The dynamic material behaviour depends on the fabrication parameters such as scanning speeds, scan pitches and scan paths. The element type used in the simulation was a 3-D cube with eight nodes. The algorithm of the dynamic finite element program is shown in **Figure 2.5**. The simulation flow procedure consisted of four.

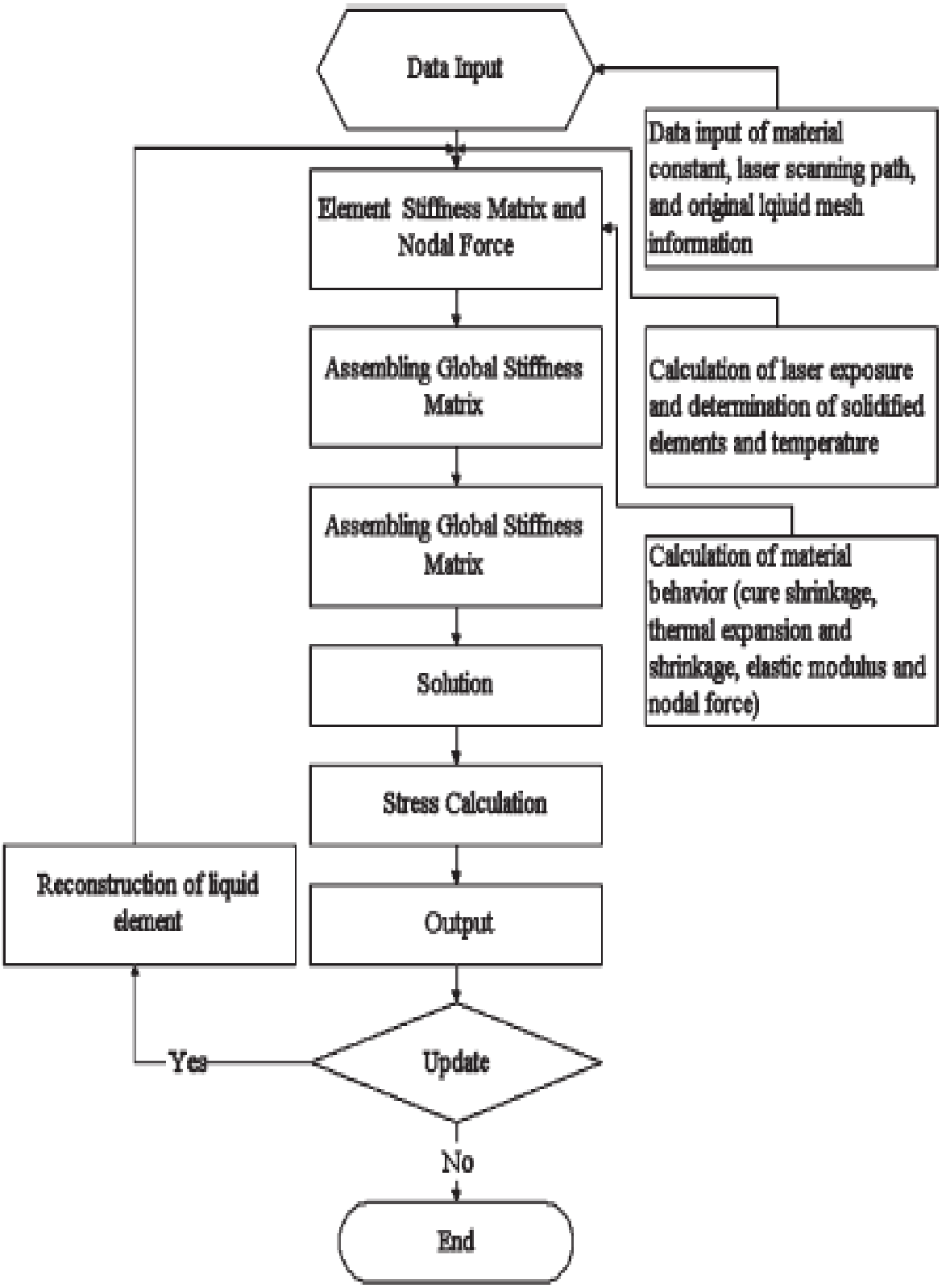

Figure 2.5 Algorithm of dynamic finite element program

parts which were pre-processing, main simulation processing, rezoning generator and post processing.The pre-processing recorded the resin properties, laser scan path as well as the coordinates and connectivity of the initial liquid nodes and element, respectively. The main simulation-processing unit handled the calculation of material behaviour, nodal force, determination of the solidified degree of element and temperature distribution. The rezoning generator handled the re-mesh problems for avoiding negative errors in the global stiffness matrix. The postprocessor gave the results and monitored the distortion behaviour.

Y.M. Huang *et. al.* [14] proposed a modified mathematical model based on reports and experimental observation of a curing process for a mask-type stereolithography system. The dominant factors of deformation were cure shrinkage, exothermic temperature variation, and swelling. All the factors occurred simultaneously during photopolymerisation. The process was a phase transition from a liquid state to a solid state and it was proved that all the factors were functions of the light exposure and elapsed time.

Dynamic Finite-Element Method

The dynamic solidification model of photopolymerisation was proposed. The constitutive equation of the mathematical model for the stereolithography process was:

$$[K]\{\Delta u\} - \{\Delta f\} = 0 \qquad \textbf{(2.53)}$$

where

$$[K] = \int_v \left[[B]^T [D][B] \right] dV \qquad \textbf{(2.54)}$$

$$\{\Delta f\} = \int_v dV \left[[B]^T \{\dot{\sigma}\} + [B]^T (3k)\{\alpha \Delta T + \Delta\beta(E)\} \right] \qquad \textbf{(2.55)}$$

In the above equation $[K]$ is the stiffness matrix, $\{\Delta u\}$ denotes the nodal displacement increment, $\{\Delta f\}$ denotes the effective nodal force increment, $[B]$ represents the strain rate–velocity matrix, $[D]$ denotes the stress–strain matrix, α denotes the linear expansion coefficient, K denotes the volume strain coefficient, ΔT denotes the temperature increment and $\Delta\beta(E)$ is defined as the strain of cure shrinkage which is a function of the laser exposure (E) and elapsed time (t).

Simulation Process

The simulation code developed for the mask-type stereolithography rapid prototyping system was based on the dynamic finite element method. The analytical process flowchart is as shown in **Figure2.6**. The element type used was a 3D cube with eight nodes. The analysis consisted of three parts: pre-processor, analytic processor, and post-processor. The pre-processor generates the required input information such as material properties, the mask geometry, nodal positions, elemental connectivity, and layer thickness. It also sliced the 3D CAD model into 2D layer data. The analytical processors handled the calculation of optical energy absorption, the determination of cure and uncure, assembling the global stiffness matrix, simulation.

Boundary Condition

The elements to be cured start to release heat during photopolymerisation, and swell by thermal expansion. The environmental temperature of the working area was also increased because of the exothermic reaction of curing the elements. Once the temperature rise stopped, the material cooled by thermal diffusion; hence, the boundary condition became an important factor in the deformation analysis.

According to the photopolymerisation process, the temperature varies linearly from T_2 to T_1 during the exothermic reaction. The constants T_2 and T_1 are represented as the maximum temperature and room temperature, respectively. The curing time for a unit element was assumed to be $n\Delta T$. It was assumed that the heating rate does not vary in the curing process. Hence, the heating rate $\dot{Q}$ can be obtained as:

$$\dot{Q} = \frac{\rho c \left(T_2 - T_1 \right)}{n \Delta t} \qquad \textbf{(2.56)}$$

where ρ and c are the density and the specific heat of the resin, respectively. The boundary conditions of the curing process are shown in **Figure2.7**. It consisted of the heat transfer to liquid resin, air, and cured elements.

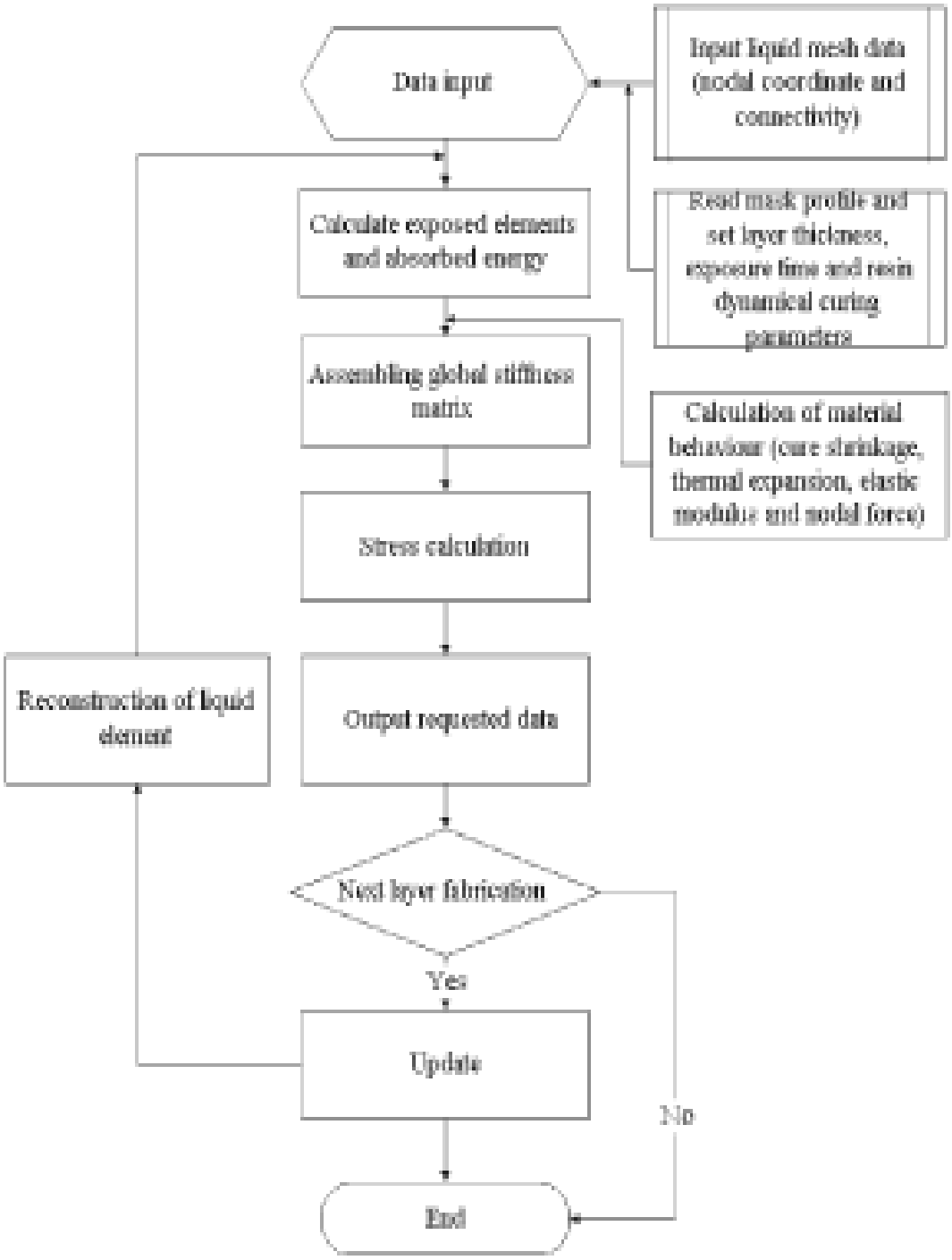

Figure 2.6 Analytical process flowchart of the developed simulation code

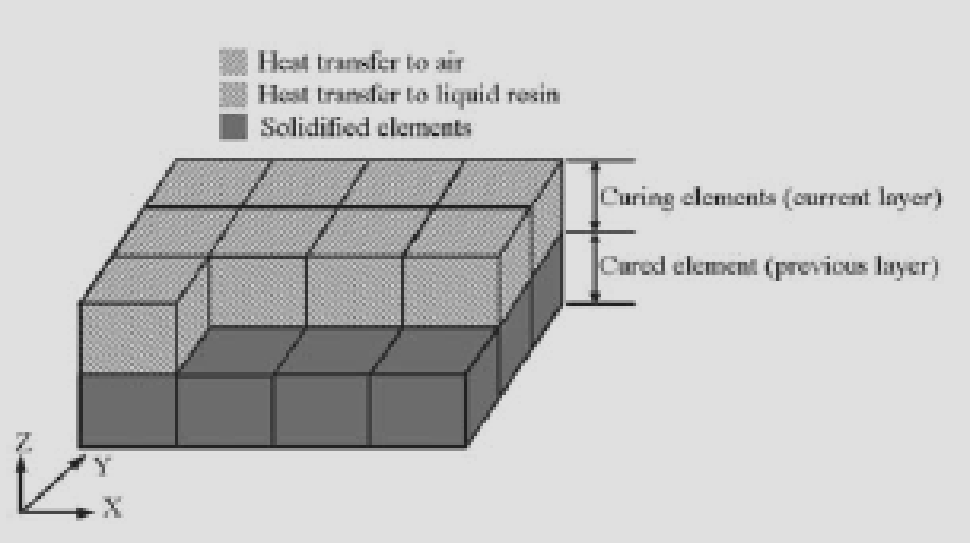

Fig. 2.7 Boundary condition of the analysis Material Properties

The increase in molecular weight and cross-linking during photopolymerisation lead to a state transition from liquid to solid. This was accompanied by a great increase of strength and was related to the conversion rate at the transition from monomer to polymer. A mathematical model of the elastic modulus was established, which is also a function of the absorption exposure energy and time. A more precise approximation formulation based on that model was proposed:

$$Y = Y_{max}\left(1 - e^{-\lambda\left(\frac{E}{E_c}-1\right)}\right)\left(1 - e^{-\alpha t}\right)\gamma \qquad \textbf{(2.57)}$$

where Y_{max} is the maximum elastic modulus of full cure and E_c is the critical exposure to produce enough free radicals to overcome oxygen inhibition and hence start the polymerization process. The constants λ and α were obtained from the experiment. The constant γ denotes the reaction coefficient of the polymerized reaction rate under exposure. In the analysis, λ and α were found to be 0.52 and 0.46, respectively, for the experimental resin NAF-202 from the Nippon Chemistry Co. From the tensile testing, the Poisson ratio was found to approach 0.3.

Y.M. Huang *et. al.* [15] proposed and described briefly the constitutive equation and modeling of the constrain surface SL system which was written and expressed as:

$$[K]\{u\} - \{f\} = 0 \qquad \textbf{(2.58)}$$

where **[**K] is the stiffness matrix, as given by equation (2.59) and **{**u} the nodal displacement vector:

$$[K] = \int_v \left[[B]^T [D][B] \right] dV \qquad \textbf{(2.59)}$$

The effective nodal force was given by

$$\{f\} = \int_v dV \left[[B]^T \{\dot{\sigma}\} + [B]^T (3K)\{\alpha \Delta T + \Delta\beta(E)\} \right] \qquad \textbf{(2.60)}$$

The element used was a cubic element with eight nodes, and the liquid element was pre-created without curing properties. The scanning path and resting time were pre-set according to the solidification process of the E-DARTS system. The constraint and boundary conditions were automatically set by determining the layer thickness. The initial nodal position, which was located at the current layer surface, was to be constrained as the same condition as the scanning process in the E-DARTS system. The boundary condition then determined which facet of the curing element was in contact with the liquid element, cured element or air. When the curing element starts to solidify, the percentage of curing degree depends on both of the absorption of energy and elapsed time. The percentage of laser exposure energy was controlled by the weight coefficient, which had a Gaussian distribution. The constraint was then released when the setting rest time was reached. The platform was lifted up above the resin surface to fill the vacant area automatically, and it was then moved down one layer thickness above the surface of resin container. The new liquid filling process was the updating of global stiffness in the developed program. The updated global stiffness matrix was another programming method in developed code.

J.D. Curtis *et. al.* [16] conducted a four-centre study in an attempt to understand the mechanisms generating, the residual birefringence associated with the stereolithographic process and investigated methodologies for producing models free of stress and

birefringence. The mechanical behavior of stereolithographic and thermo-setting resins was compared at room temperature and under stress-freezing conditions.

Jeffrey Stansbury *et. al.* [17] reviewed that polymerization of conventional monomers, whether initiated thermally, photochemically or by some other means, results in a significant reduction in volume that causes difficulties in many polymer applications. The stress that arises during polymerization generates either internal or interfacial defects as well as substrate deformation. This brief review seeks to outline some of the shrinkage and stress related issues that are relevant to the photopolymerization of unfilled resins and composites. Methods used to measure shrinkage and stress were described and some of the materials approaches were developed to minimize these factors.

Y.-M. Huang *et. al.* [18] reviewed that stereolithography (SL) technology can be classified into two types, free-surface and the constrain surface SL systems. Constrain-surface stereolithography (SL) systems have the advantages of resin savings, reduced cost and better layer thickness control. However, the material properties of the curing process and the fabrication parameters need to be determined and optimal process parameters should be found using numerical analysis in order to eliminate trial and error. This paper reported some fundamental experiments that were conducted in order to explore the curing properties of the resin NAF202 in an E-DARTS system. In addition, a theoretical analysis of the photopolymer curing process in the E-DARTS system was proposed. A dynamic finite element simulation code with weight function was developed to model the point-by point curing process in a constrained-surface SL system. A simple implementation to evaluate the developed program was also presented, indicating that the proposed program can simulate the shrinkage analysis in accordance with path planning.

R. HAGUE *et. al.* [19] summoned significant initial investigations into the properties of Accura SI40 and SL7560 resins which represent two state of the art stereolithography resins that were aimed at end-use part manufacture. This information was previously been unavailable and was vital for their consideration in end-use part manufacture. The impact of various levels of post curing (ultraviolet and thermal) on the tensile, flexural

and impact properties were investigated and correlated with differential scanning calorimetry (DSC) analysis. The isotropy/anisotropy nature of the two materials and also the effect of the notch creation method on the impact resistance were also studied.

Wenbin Hong *et. al.* [20] presented a thermal analysis of forming the top layer of a five-layer part made using a stepless rapid prototyping process, which cures successive layers of liquid polymer through exposure to UV light. A computer model was created to simulate the kinetics of the UV light induced photo-polymerization; the heat transfer in the curing stage and the process after UV curing was established. A temperature profile in the UV curing was obtained through the simulation. It was found that temperature in the top layer rose very rapidly upon exposure to the UV radiation, and reached the maximum point near 100 degree centigrade at the end of curing. After the UV lamp was turned off, the layer temperature dropped quickly to room temperature due to convection. An in situ 2D thermal imaging experiment was conducted to verify the simulation results. It showed that the modeling agreed well with the experimental results.

Y.M. Huang *et. al.* [21] proposed a modified mathematical model based on the experimental observations of the curing process for mask-type stereolithographic systems. This process is a phase transition from the liquid state to the solid state, proving that all factors are functions of the duration of the exposure to light, and the intensity of that light.

Dynamic finite element method

A dynamic solidification model of photo-polymerization was proposed which explained that the behavior of the cure resin is a function of the intensity of that light I and the elapsed time t . The uncured liquid becomes more viscous as it absorbs the heat produced by the cured resin. For the convenience to express, a substitution as the strain rate $\{\dot{\varepsilon}\}$ for the increment of strain $\{\Delta\varepsilon\}$ was taken. Therefore, the deformation of resin consists of the following elements

$$\{\dot{\varepsilon}\} = \{\dot{\varepsilon}^{e}\} + \{\dot{\varepsilon}^{T}\} + \{\dot{\varepsilon}^{v}\} + \{\dot{\varepsilon}^{\gamma}\} + \{\dot{\varepsilon}^{p}\} \qquad \textbf{(2.61)}$$

where $\{\dot{\varepsilon}^e\}$ represents the elastic strain rate; $\{\dot{\varepsilon}^v\}$ is the viscous strain rate that is the function of time, so it was expressed as $\{\sigma(t)\}$; $\sigma(t)$ is the viscous stress that is the function of time (t); $\{\dot{\varepsilon}^T\}$ is the thermal strain rate that was rewritten as $\{\alpha\dot{T}\}$; $\{\dot{\varepsilon}^\gamma\}$ is the strain rate caused by cure shrinkage and is given by $\Delta\beta(I,t)$ and $\{\dot{\varepsilon}^p\}$ is the plastic strain rate. During photo-polymerization, the plastic strain is low and can be neglected. In the case in which $\{\dot{\sigma}\}$ equals $[D^e]\{\dot{\varepsilon}\}$ and $\{\dot{\varepsilon}\}$ equals $[B]\{u\}$, substituting the above relationship and $\int_v [B]^T dV$ into Eq. (1), yields the following equation:

$$\int_v \left[[B]^T [D^e] [B] \{\dot{u}\} - [B]^T \{\sigma\} - [B]^T (3K)\{\alpha \Delta \dot{T} + \Delta\beta(I)\} \right] dV = 0 \quad \textbf{(2.62)}$$

Consequently, the constitutive equation in the dynamic finite element analysis of the stereolithographic process can be expressed as:

$$[K]\{\dot{u}\} - \{\dot{f}\} = 0 \quad \textbf{(2.63)}$$

Where $$[K] = \int_v \left[[B]^T [D^e] [B] \right] dV \quad \textbf{(2.64)}$$

$$\{\dot{f}\} = \int_v \left[[B]^T \{\sigma\} + [B]^T (3k)\{\alpha \Delta \dot{T} + \Delta\beta(I)\} \right] dV \quad \textbf{(2.65)}$$

In the above equation, $[K]$ is the stiffness matrix; $\{\dot{u}\}$ is the increment in nodal displacement; $\{\dot{f}\}$ is increment in the effective nodal force; $[B]$ represents the strain rate–velocity matrix; $[B]^T$ is the transpose of the matrix $[B]$; $[D^e]$ is the stress–strain matrix; V is the volume of the reaction area; $\{\sigma\}$ represents the nodal viscous stress that is the function of time (t); k is the volume modulus; α is the linear expansion coefficient; $\dot{T}$ is the increment in temperature, and $\Delta\beta(I)$ is defined as the strain associated with cure shrinkage, which is a function of the intensity of that light (I) and elapsed time (t).

Energy distribution in mask type prototyping

As light passes through the mask onto the surface of the resin, the distribution and uniformity of the diffusion of the energy on the surface affects the thickness of solidified layers. Therefore, the energy of the light that passes through the mask and is projected onto the surface of the resin must be calculated using a mathematical model to determine the energy of the mask. A square of side 'a' is considered as an example. The energy intensity of the light source is I_0 .The central point of the square mask is defined as $x = 0$ and $y = 0$ .After the light had passed through the mask, the intensity at any point in the square profile is given by:

$$I_d = \frac{1}{4} I_0 \left(C_x^2 C_x^2 + C_x^2 S_x^2 + S_x^2 C_y^2 + S_x^2 S_y^2 \right) \quad \textbf{(2.66)}$$

where the relative coefficients, C and S, are defined as follows:

$$C_x = \int_{p_1}^{p_2} \cos\left(0.5\pi u^2\right) du \quad \textbf{(2.67)}$$

$$S_x = \int_{p_1}^{p_2} \sin\left(0.5\pi u^2\right) du \quad \textbf{(2.68)}$$

$$C_y = \int_{q_1}^{q_2} \cos\left(0.5\pi u^2\right) du \quad \textbf{(2.69)}$$

$$S_x = \int_{q_1}^{q_2} \sin\left(0.5\pi u^2\right) du \quad \textbf{(2.70)}$$

where

$$p_1 = \frac{2}{\sqrt{m}}\left(\frac{x}{a} - 0.5\right) \quad \textbf{(2.71)}$$

$$p_2 = \frac{2}{\sqrt{m}}\left(\frac{x}{a} - 0.5\right) \quad \textbf{(2.72)}$$

$$q_1 = \frac{2}{\sqrt{m}}\left(\frac{y}{a} - 0.5\right) \quad \textbf{(2.73)}$$

$$q_2 = \frac{2}{\sqrt{m}}\left(\frac{y}{a} - 0.5\right) \quad \textbf{(2.74)}$$

and

$$m = \frac{2\lambda(b - z)}{a^2} \quad \textbf{(2.75)}$$

where λ is the wavelength of light, and b represents the distance between the resin surface and the light mask. Hence, based on the Beer–Lambert Law, the equation that specifies the light energy absorbed by the resin is,

$$I(x, y, z) = I_d(x, y, z)e^{-\varphi z} \quad \textbf{(2.76)}$$

where φ is the rate of absorption of wavelength λ by the resin. Thus, the energy to which every point is exposed is given by $E(x,y,z) = I(x,y,z)t$, where t is the period of exposure.

DFEM simulation

A cubic element with eight nodes is used to reflect realistically the characteristics of the RP layer. The developed simulation code is based on the dynamic finite element method. **Figure 2.8** shows a flowchart of the simulation process. The liquid mesh is pre-created and read into a matrix core, of an ‘‘H-4’’ diagnostic part. This study involved 1680 elements and 2366 nodes. **Table 2.1** presents the parameters used in the simulation. The simulation of the DFEM yields the displacement of every node of the part. This information can be used to improve the profile of the part after deformation, and yield the new matrix of every node after compensation.

Table 2.1 Parameters of experiment and simulation

Part	Element number	Node number	Thickness (mm)	Layer	Exposure time (s)	Simulation time (min)
H-4 part	1680	2366	0.1	150	10	150

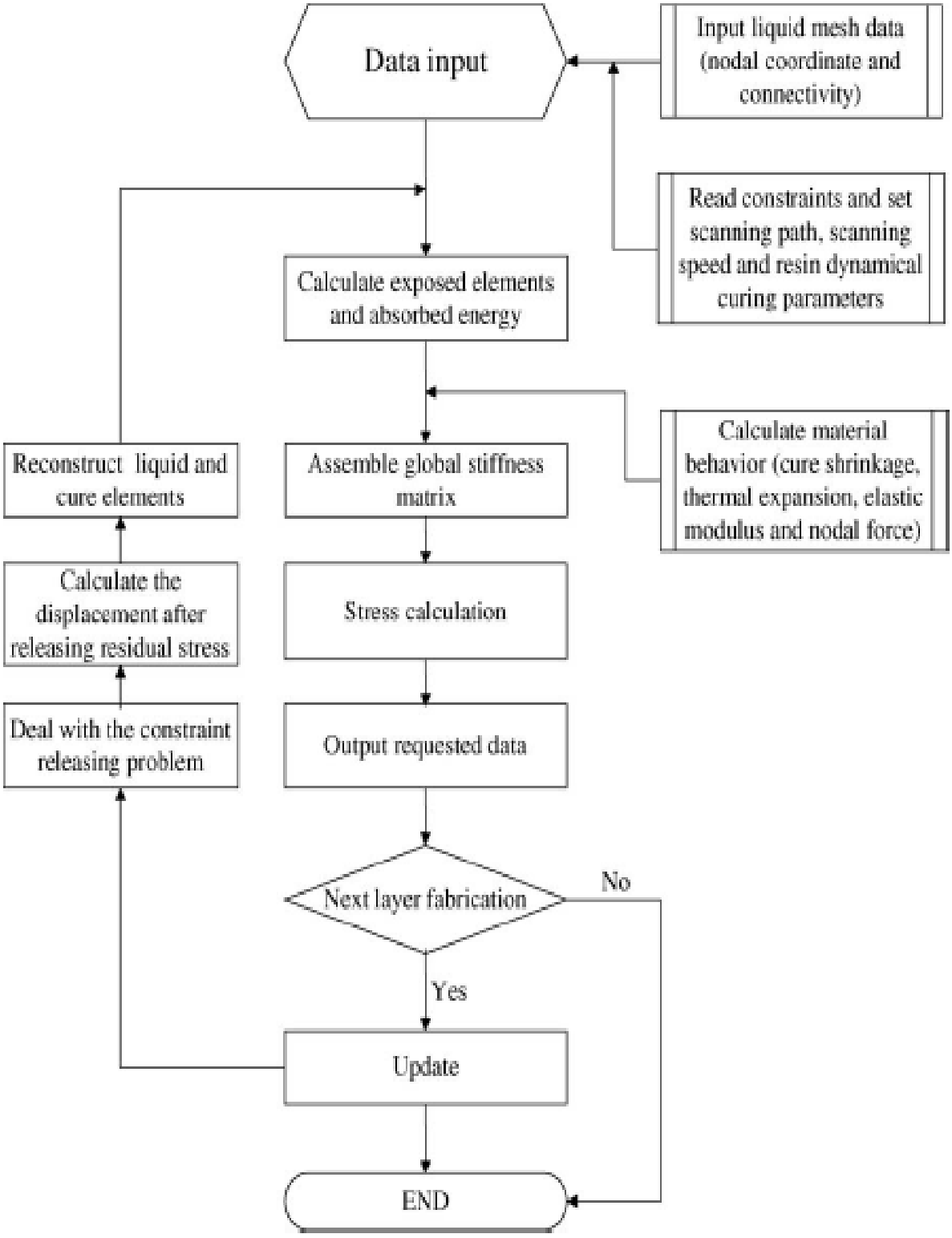

Figure 2.8 Flowchart of the simulation process

You-Min Huang *et. al.* [22] studied that rapid prototyping (RP) is a fast and feasible technique for prototype construction. However, the phenomenon of volume shrinkage is unavoidable with any material or building method. The volume shrinkage and curl distortion are the main reason for the inaccuracy of the built prototype. The curl distortion changes with the laser scan path; the curl distortion increases with both scanning length and part height. Consequently, the error is serious for built prototypes with parts that have large height–length dimensions. Subsequently, more expensive equipment is used to improve the precision of the dimension and volume shrinkage on the market. Also, obtaining better processes parameters via trial and error in the RP process is expensive and inefficient. In order to improve dimension precision, and reduce the processing cost and the frequency of trial and error, this study first induced the concept of CAE into the processing of RP, which uses a dynamic finite element simulation code to simulate the photopolymerization process, to reduce the selection time for the processing parameters and obtain the distortion data. Second, dynamic reverse compensation employed to obtain a new CAD model, which is then loaded into a RP machine for practical prototype processing, to increase the accuracy of the process. Finally, to confirm this method and restriction in experimental equipment, stereolithography process and simple laser scanning path were chosen as examples for experimental comparison. The results of the simulation and experiment demonstrate the effectiveness of the proposed method. The proposed method cannot only reduce the equipment cost but also can simultaneously enhanced precision of the dimensions of the final parts. Besides, this method was believed to be applicable to other materials or build-up methods used in RP fabrication.

You-Min Huang *et. al.* [23] quoted that the rapid prototyping (RP) process is the fastest and most feasible method for prototype construction. However, with the use of any material or build method the phenomenon of volume shrinkage is unavoidable. It is known that volume shrinkage and curl distortion are the major causes that lead to poor accuracy of the built prototype. Subsequently, in order to improve the precision of dimension and volume shrinkage, more expensive equipment is used on the market. Also, it is expensive and inefficient to obtain better process parameters through trail and error

in the RP process. In order to improve the precision of dimension, reduce the processing cost and the frequency of trail and error, this study first induces the concept of computer aided engineering (CAE) into the processing of RP, which uses a dynamic finite element simulation code to simulate the photopolymerization process, so as to reduce the time for selecting the processing parameters and obtain the distortion data. Second, by means of reverse distortion compensation to obtain a new CAD model, then it is sent to a RP machine for the actual prototyping processes, so as to obtain a more accurate precision. Finally, in order to confirm this method and restriction in experimental equipment, the stereolithography process and simple laser scanning path are chosen as examples. The results of the simulation and experiment prove that the method proposed herein is effective. It not only can reduce the cost of equipment but also obtain a better precision of dimension on final-parts at the same time. Besides, it is believed that this research method can be promoted to other materials or build methods in RP fabrication.

Cho-Pei Jiang *et. al.* [24] aimed to introduce the principle of the mask exposure and scanning stereolithography (MESS) and to develop a simulation code to analyze the MESS process. It was studied that photopolymerization is a key reaction in stereolithography. It brings about molecular linkage and releases exothermic temperature. The shrinkage effect is the major cause of prototype deformation, and the shrinkage resulting from scanning and mask exposing is different. It is important to analyze the inaccuracy of each curing layer after the mask exposing in order to optimize the scanning parameters. A simulation code, based on dynamic finite element method, to analyze the shrinkage effect in accordance with scanning path and mask exposure pattern was used. A benchmark model was proposed to validate the implementation of the developed code. The simulation results showed that the developed code can analyze the deformation in laser scanning, masking exposing and the MESS process. In benchmark model study, the sharp corner shrinks faster than rounded edge in mask pattern curing. Although the profile scanning can maintain the high accuracy in the MESS process, the residual stress can be easily discovered inside of the sharp corner. And it was believed that the developed simulation code can be applied for optimizing scan path and exposing time

due to the analysis process in accordance with the drawing path and fabrication parameters.

Yuung-Hwa *et. al.* [25] developed a FORTRAN program to convert the explicit dynamic finite element method (FEM) simulated deformed sheet to the stereolithography (STL) format used in the rapid prototyping (RP) apparatus. And stated that such an integration of the RP/FEM can rapidly produce a visualized 3D physical part of the sheet deformation state. Three cases – cylindrical drawing bore expanding and square cup drawing processes, simulated by explicit dynamic FEM – were investigated to verify the integration system. The wrinkled flange in the cylindrical drawing process, the circle hole expansion in the bore expanding process, and the square cup in the square cup drawing were successfully predicted by explicit dynamic FEM, and the rapid prototyping 3D physical parts also showed good visualization of the deformed sheet for the above three cases. It was proved that the integration system of RP/FEM will be able to supply a useful method for the visualization of the 3D physical part in the sheet metal forming process.

K. Chockalingam *et. al.* [26] reviewed that rapid prototyping (RP) is an emerging technology that has been implemented in many spheres of industry particularly in the area of new product development. Growth of this field has been rapid in recent years. Stereolithography (SL) is one of the most popular RP process used for rapid tooling applications. There are several process parameters contributing to the strength of an SL product. The contribution of three parameters; namely, layer thickness, post curing time and orientation are most significant. In light of this concern, an attempt was made to study and optimize these process parameters for maximum part strength, and develop an empirical relationship between process parameters and part strength through design of experiments (DOE). The proposed DOE was verified with the data of experiments conducted under standard conditions.

You-Min Huang *et. al.* [27] studied that stereolithography (SL) is one of the rapid prototyping (RP) systems that use liquid photopolymer resin as the raw material for

building prototypes. The photopolymer type of the RP system employs lasers to selectively expose the surface of the liquid resin. The absorbance of energy leads to photo-polymerization that transfers the liquid resin into solid. Subsequently, the phenomenon of volume shrinkage is unavoidable, and the curl distortion changes with the different laser scan paths, even affecting the geometric profile of the final-parts. The volume shrinkage and curl distortion are the major causes that lead to poor accuracy of the built prototype. In order to understand and improve the curl distortion and the geometric profile, so as to find a simple and suitable laser scan path this paper first of all used simulation and experiment to explore the deformation and shrinkage during the process of photo-polymerization while the liquid resin uses a laser beam to carry out single line scanning or single layer scanning in liquid free surface, and further understands the final change of geometric profile. Secondly, it investigated into the curl distortion and changes of geometric profile occurred in the three-dimensional part by different scan paths. Finally, a simple, proper, and effective laser scan path planning was suggested to decrease the curl distortion, and promote the dimension accuracy and the profile of the final-parts. Besides, this paper also mentions the feasibility of multi-optical processing.

D.E. Karalekas *et. al.* [28] based their study to evaluate the feasibility of a commercially available epoxy-based photopolymer for photoelastic investigations. A number of experiments were undertaken to address critical material and fabrication issues related to stereolithography built photoelastic specimens. The data gathered from photoelastic model testing was compared to the ones generated by numerical analysis. The good correlation between them in terms of measured and calculated magnitudes of stress provided increased confidence in the investigated photopolymer for photoelastic stress analysis purposes, and consequently for validation of computer-based models, utilizing these stereolithography models as complementary design tools.

Fernand Ellyin *et. al.* [29] studied that stereolithography (SLA) is a technique which uses a laser beam to cure a photopolymer liquid resin with three dimensional computer-aided design (CAD) data. The accuracy of the prototype, the build time, and the cured

properties of the resins are controlled by the SLA process parameters such as the size of the laser beam, scan velocity, hatch spacing, and layer thickness. In particular, the size of the laser beam is the most important parameter in SLA. This study investigated the curing properties of photopolymers as a function of the laser beam size. The cure width and depth were measured either on a single cure line or at a single cure layer for various hatch spacings and laser beam sizes. The cure depth ranged from 0.23 to 0.34 mm and was directly proportional to the beam radius, whereas the cure width ranged from 0.42 to 1.07 mm and was inversely proportional to the beam radius. The resulting surface roughness ranged from 1.12 to 2.23 μm for a ratio of hatch spacing to beam radius in the range 0.5–2.0 at a beam radius of 0.17 mm and a scan velocity of 125 mm/sec.

Jae-Hyung Sim *et. al.* [30] presented a nonlinear viscoelastic constitutive model, in differential form, based on the deformation characteristics of thermoset polymers under complex loadings. This rheological model included a criterion to delineate loading and unloading in multiaxial stress states, and different moduli for loading and unloading behaviors. The material constants and functions of this model were calibrated in accordance with a well-defined procedure. The model predictions were compared with the experimental data of an epoxy polymer subjected to uniaxial and biaxial stress states with monotonic and cyclic loading. The agreement was very good for various loading regimes. The constitutive model was further implemented in a finite element code and the residual stresses arising from the curing process of polymer reinforced composites were determined for two different epoxy resins.

CHAPTER-3 ANALYTICAL FORMULATION

In order to realistically reflect the characteristics of the RP layer build, the element used is a cubic element with eight nodes, so for analytical formulation the formula's according to Serendipity family for eight noded element are given by:

$$N_i = \frac{1}{8}(1+\varepsilon_0)(1+\eta_0)(1+\rho_0) \tag{3.1}$$

where N_i is the shape function;

Where $$\varepsilon_0 = \varepsilon * \varepsilon_i \tag{3.2}$$

$$\eta_0 = \eta * \eta_i \tag{3.3}$$

$$\rho_0 = \rho * \rho_i \tag{3.4}$$

where ε_i , η_i, ρ_i are general co-ordinates of eight noded element having value in terms of ± 1 with respect to the center ε , η, ρ which is at $(0,0,0)$

$$J = \begin{bmatrix} \sum_{i=1}^{n} \frac{dN_i}{d\varepsilon} x_i & \sum_{i=1}^{n} \frac{dN_i}{d\varepsilon} y_i & \sum_{i=1}^{n} \frac{dN_i}{d\varepsilon} z_i \\ \sum_{i=1}^{n} \frac{dN_i}{d\eta} x_i & \sum_{i=1}^{n} \frac{dN_i}{d\eta} y_i & \sum_{i=1}^{n} \frac{dN_i}{d\eta} z_i \\ \sum_{i=1}^{n} \frac{dN_i}{d\rho} x_i & \sum_{i=1}^{n} \frac{dN_i}{d\rho} y_i & \sum_{i=1}^{n} \frac{dN_i}{d\rho} z_i \end{bmatrix} \tag{3.5}$$

where J is the Jacobien matrix;

n is the number of nodes;

x_i , y_i, z_i are the co-ordinates of the nodes of elements of the prototype which is to be meshed meshed into general eight noded elements;

$$[B]_{x,y,z} = J^{-1} * [B]_{\varepsilon,\eta,\rho} \tag{3.6}$$

where $[B]_{x,y,z}$ is strain rate–velocity matrix matrix of order $[6*24]$ in x , y , z co-ordinates;

J^{-1} is inverse of Jacobien matrix

$[B]_{\varepsilon,\eta,\rho}$ is strain rate–velocity matrix matrix of order $[6*24]$ in ε , η , ρ co-ordinates;

For convenience to express, the strain rate $\{\dot{\varepsilon}\}$ is substituted for the increment of strain $\{\Delta\varepsilon\}$.

3.1 For elastic materials

From elastic Hooke's law

$$\{\dot{\varepsilon}^e\} = [C^e]\{\dot{\sigma}\}, \quad \{\dot{\sigma}\} = [D^e]\{\dot{\varepsilon}^e\} \tag{3.7}$$

and

$$[C^e] = \frac{1}{E}\begin{bmatrix} 1 & -\mu & -\mu & 0 & 0 & 0 \\ -\mu & 1 & -\mu & 0 & 0 & 0 \\ -\mu & -\mu & 1 & 0 & 0 & 0 \\ 0 & 0 & 0 & 2(1+\mu) & 0 & 0 \\ 0 & 0 & 0 & 0 & 2(1+\mu) & 0 \\ 0 & 0 & 0 & 0 & 0 & 2(1+\mu) \end{bmatrix} \tag{3.8}$$

$$[D^e] = [C^e]^{-1} = \frac{E}{1+\mu}\begin{bmatrix} \frac{1-\mu}{1-2\mu} & \frac{\mu}{1-2\mu} & \frac{\mu}{1-2\mu} & 0 & 0 & 0 \\ \frac{\mu}{1-2\mu} & \frac{1-\mu}{1-2\mu} & \frac{\mu}{1-2\mu} & 0 & 0 & 0 \\ \frac{\mu}{1-2\mu} & \frac{\mu}{1-2\mu} & \frac{1-\mu}{1-2\mu} & 0 & 0 & 0 \\ 0 & 0 & 0 & \frac{1}{2} & 0 & 0 \\ 0 & 0 & 0 & 0 & \frac{1}{2} & 0 \\ 0 & 0 & 0 & 0 & 0 & \frac{1}{2} \end{bmatrix} \tag{3.9}$$

for example

$$\dot{\varepsilon}_x^e = \frac{1}{E}\left[\dot{\sigma}_x - \mu\left(\dot{\sigma}_y + \dot{\sigma}_z\right)\right] \tag{3.10}$$

$$\dot{\varepsilon}_y^e = \frac{1}{E}\left[\dot{\sigma}_y - \mu\left(\dot{\sigma}_z + \dot{\sigma}_x\right)\right] \tag{3.11}$$

$$\dot{\varepsilon}_z^e = \frac{1}{E}\left[\dot{\sigma}_z - \mu\left(\dot{\sigma}_x + \dot{\sigma}_y\right)\right] \tag{3.12}$$

and

$$\dot{\varepsilon}_k = \dot{\varepsilon}_x^e + \dot{\varepsilon}_y^e + \dot{\varepsilon}_z^e = \frac{1-2\mu}{E}\left(\dot{\sigma}_x + \dot{\sigma}_y + \dot{\sigma}_z\right) \quad \textbf{(3.13)}$$

$$G = \frac{E}{2(1+\mu)} \quad \textbf{(3.14)}$$

$$k = \frac{E}{3(1-2\mu)} \quad \textbf{(3.15)}$$

where $\{\dot{\varepsilon}^e\}$ represents the elastic strain rate; $\{\dot{\sigma}\}$ is the stress rate; $[C^e]$ is the elastic flexibility matrix ; $[D^e]$ is the elastic stress-strain matrix; $\dot{\varepsilon}_k$ is the volume strain rate; E is the elastic modulus; μ is the poisson's ratio; G is the shear modulus; k is the volume modulus.

3.2 For viscous-elastic-plastic materials

Constitutive equations of Maxwell model for viscous-elastic-plastic materials are expressed by:

$$\{\dot{\varepsilon}\} = \{\dot{\varepsilon}^e\} + \{\dot{\varepsilon}^T\} + \{\dot{\varepsilon}^V\} + \{\dot{\varepsilon}^\gamma\} + \{\dot{\varepsilon}^p\} \quad \textbf{(3.16)}$$

During photo-polymerization the plastic strain rate $\{\dot{\varepsilon}^p\}$ is low and can be neglected. Thus, equation. (3.16) can be rewritten as:

$$\{\dot{\varepsilon}\} = \{\dot{\varepsilon}^e\} + \{\dot{\varepsilon}^T\} + \{\dot{\varepsilon}^V\} + \{\dot{\varepsilon}^\gamma\} \quad \textbf{(3.17)}$$

and

$$\{\dot{\varepsilon}^V\} = \{\dot{\varepsilon}^d\} + \{\dot{\varepsilon}^k\} = \frac{1}{2\eta_G}\{\sigma'\} + \frac{1}{3\eta_k}\{\sigma_m\} \quad \textbf{(3.18)}$$

$$t_G = \frac{\eta_G}{G}, \quad t_k = \frac{\eta_k}{k} \quad \textbf{(3.19)}$$

$$\sigma_x' = \frac{1}{3}\left(2\sigma_x - \sigma_y - \sigma_z\right), \quad \sigma_y' = \frac{1}{3}\left(2\sigma_y - \sigma_z - \sigma_x\right), \quad \sigma_z' = \frac{1}{3}\left(2\sigma_z - \sigma_x - \sigma_y\right) \quad \textbf{(3.20)}$$

$$\sigma_m = \frac{1}{3}\left(\sigma_x + \sigma_y + \sigma_z\right) \quad \textbf{(3.21)}$$

where $\{\dot{\varepsilon}\}$ is the Euler strain rate; $\{\dot{\varepsilon}^e\}$ represents the elastic strain rate; $\{\dot{\varepsilon}^T\}$ is the thermal strain rate that can be rewritten as $\{\alpha\dot{T}\}$; $\{\dot{\varepsilon}^V\}$ is the viscous strain rate that is

the function of time, so it can be expressed a $\{\sigma(t)\}$[11]; $\sigma(t)$ represents the nodal viscous stress that is the function of time (t); $\{\dot{\varepsilon}^{\gamma}\}$ is the strain rate caused by cure shrinkage and is given by $\{\Delta\beta(I,t)\}$,which is a function of intensity of light (I) and the elapsed time (t); $\{\dot{\varepsilon}^{d}\}$ and $\{\dot{\varepsilon}^{k}\}$ are two components of viscous strain rate $\{\dot{\varepsilon}^{V}\}$ in the shear component and volume component relatively; η_G and η_k are the viscous coefficient in the shear deformation and volume deformation relatively; G is the shear modulus; k is the volume modulus; t_G and t_k are the slack time relatively G and k ; σ' is the deviatoric stress; σ_m is the mean stress. By substituting equation (3.18) into (3.17), yields the following equation:

$$\begin{Bmatrix}\dot{\varepsilon}_x\\ \dot{\varepsilon}_y\\ \dot{\varepsilon}_z\\ \dot{\gamma}_{yz}\\ \dot{\gamma}_{zx}\\ \dot{\gamma}_{xy}\end{Bmatrix}=\begin{Bmatrix}\dot{\varepsilon}_x^e\\ \dot{\varepsilon}_y^e\\ \dot{\varepsilon}_z^e\\ \dot{\gamma}_{yz}^e\\ \dot{\gamma}_{zx}^e\\ \dot{\gamma}_{xy}^e\end{Bmatrix}+\begin{Bmatrix}\alpha\dot{T}\\ \alpha\dot{T}\\ \alpha\dot{T}\\ 0\\ 0\\ 0\end{Bmatrix}+\frac{1}{2\eta_G}\begin{Bmatrix}\sigma'_x\\ \sigma'_y\\ \sigma'_z\\ 2\tau_{yz}\\ 2\tau_{zx}\\ 2\tau_{xy}\end{Bmatrix}+\frac{1}{3\eta_k}\begin{Bmatrix}\sigma_m\\ \sigma_m\\ \sigma_m\\ 0\\ 0\\ 0\end{Bmatrix}+\begin{Bmatrix}\Delta\beta(I)\\ \Delta\beta(I)\\ \Delta\beta(I)\\ 0\\ 0\\ 0\end{Bmatrix} \qquad \textbf{(3.22)}$$

substituting equations (3.20), (3.21) into (3.22), yields the following equation:

$$\begin{Bmatrix}\dot{\varepsilon}_x^e\\ \dot{\varepsilon}_y^e\\ \dot{\varepsilon}_z^e\\ \dot{\gamma}_{yz}^e\\ \dot{\gamma}_{zx}^e\\ \dot{\gamma}_{xy}^e\end{Bmatrix}=\begin{Bmatrix}\dot{\varepsilon}_x\\ \dot{\varepsilon}_y\\ \dot{\varepsilon}_z\\ \dot{\gamma}_{yz}\\ \dot{\gamma}_{zx}\\ \dot{\gamma}_{xy}\end{Bmatrix}-\begin{Bmatrix}\alpha\dot{T}\\ \alpha\dot{T}\\ \alpha\dot{T}\\ 0\\ 0\\ 0\end{Bmatrix}-\left[D^{\eta\kappa}\right]\begin{Bmatrix}\sigma_x\\ \sigma_y\\ \sigma_z\\ \tau_{yz}\\ \tau_{zx}\\ \tau_{xy}\end{Bmatrix}-\begin{Bmatrix}\Delta\beta(I)\\ \Delta\beta(I)\\ \Delta\beta(I)\\ 0\\ 0\\ 0\end{Bmatrix} \qquad \textbf{(3.23)}$$

where

$$\left[D^{\eta\kappa}\right]=\frac{1}{18\eta_G\eta_k}\begin{bmatrix}2\eta_G+6\eta_k & & & & & & \\ 2\eta_G-3\eta_k & 2\eta_G+6\eta_k & & \textit{symetric} & & & \\ 2\eta_G-3\eta_k & 2\eta_G-6\eta_k & 2\eta_G+6\eta_k & & & & \\ 0 & 0 & 0 & 18\eta_k & & & \\ 0 & 0 & 0 & 0 & 18\eta_k & & \\ 0 & 0 & 0 & 0 & 0 & 18\eta_k & \\ 0 & 0 & 0 & 0 & 0 & 0 & 18\eta_k\end{bmatrix}$$

substituting Eqs. (3.19), (3.23) into (3.7), yields the following equation:

$$\begin{Bmatrix} \dot{\sigma}_x \\ \dot{\sigma}_x \\ \dot{\sigma}_x \\ \dot{\tau}_{yz} \\ \dot{\tau}_{yz} \\ \dot{\tau}_{yz} \end{Bmatrix} = \left[D^e\right] \begin{Bmatrix} \dot{\varepsilon}_x \\ \dot{\varepsilon}_y \\ \dot{\varepsilon}_z \\ \dot{\gamma}_{yz} \\ \dot{\gamma}_{zx} \\ \dot{\gamma}_{xy} \end{Bmatrix} - \frac{E}{1-2\mu} \begin{Bmatrix} \alpha\dot{T} \\ \alpha\dot{T} \\ \alpha\dot{T} \\ 0 \\ 0 \\ 0 \end{Bmatrix} - \left[t^{\eta\kappa}\right] \begin{Bmatrix} \sigma_x \\ \sigma_y \\ \sigma_z \\ \tau_{yz} \\ \tau_{zx} \\ \tau_{xy} \end{Bmatrix} - \frac{E}{1-2\mu} \begin{Bmatrix} \Delta\beta(I) \\ \Delta\beta(I) \\ \Delta\beta(I) \\ 0 \\ 0 \\ 0 \end{Bmatrix} \tag{3.24}$$

and

$$\left[t^{\eta\kappa}\right] = \begin{bmatrix} t_G + 2t_k & & & & & \\ t_G - t_k & t_G + 2t_k & & symmetric & & \\ t_G - t_k & t_G - t_k & t_G + 2t_k & & & \\ 0 & 0 & 0 & 3t_k & & \\ 0 & 0 & 0 & 0 & 3t_k & \\ 0 & 0 & 0 & 0 & 0 & 3t_k \end{bmatrix} \tag{3.25}$$

where $\left[t^{\eta\kappa}\right]$ is the slack time matrix that is the function of time(t), so $\left\{\dot{\varepsilon}^V\right\}$ it can be expressed as $\{\sigma(t)\}$ [11], where σ represents the nodal viscous stress that is the function of time (t) .

Substituting Eq. (A6) into (3.15) thus (3.15) can be written as:

$$\left\{\dot{\sigma}\right\} = \left[D^e\right]\left\{\dot{\varepsilon}\right\} - 3k\left\{\alpha\dot{T}\right\} - \left\{\sigma(t)\right\} - 3k\left\{\Delta\beta(I)\right\} \tag{3.26}$$

Matching the relation of finite elements:

$$\{\dot{\varepsilon}\} = [B]\{\dot{u}\} \tag{3.27}$$

substituting Eqs. (3.20) into (3.19) and $\int_v [B]^T dV$ into virtual work principle, yields the following equation for viscous-elastic-plastic materials is expressed as:

$$\int_v [\delta\dot{e}]\{\sigma\}\, dV = \int_v \begin{bmatrix} [B]^T \left[D^e\right][B]\{\dot{u}\} - [B]^T \{\sigma\} \\ -[B]^T (3k)\{\alpha\dot{T} + \Delta\beta(I)\} \end{bmatrix} dV = 0 \tag{3.28}$$

Consequently, the constitutive equation in the finite element analysis of the sterolithography process can be expressed as:

$$[k]\{\dot{u}\} - \{\dot{f}\} = 0 \tag{3.29}$$

where

$$[k] = \int_v [B]^T [D^e][B] dV \tag{3.30}$$

$$\{\dot{f}\} = \int_v \left[[B]^T \{\sigma\} - [B]^T (3k)\{\alpha \dot{T} + \Delta\beta(I)\} \right] dV \tag{3.31}$$

$[k]$ is the stiffness matrix; $\{\dot{u}\}$ is the increment in nodal displacement; $\{\dot{f}\}$ is increment in the effective nodal force; $[B]$ represents the strain rate–velocity matrix; $[B]^T$ is the transpose of the matrix $[B]$; $[D^e]$ is the stress–strain matrix; V is the volume of the reaction area; $\{\sigma\}$ represents the nodal viscous stress that is the function of time (t); k is the volume modulus; α is the linear expansion coefficient; $\dot{T}$ is the increment in temperature, and $\Delta\beta(I)$ is defined as the strain associated with cure shrinkage, which is a function of the intensity of that light (I) and elapsed time (t).

CHAPTER-4 PROBLEM FORMULATION

4.1Algorithm for problem formulation:

The developed simulation code is based on the finite element method, and the flowchart of the simulation process is shown in Figure 4.3. The liquid mesh is pre-created and read into the matrix core using the ANSYS software. In order to realistically reflect the characteristics of the RP layer build and the phenomenon of laser path scanning, the element used is a cubic element with eight nodes as shown in **Figure 4.1** that is SOLID45, 3-D, Structural Solid. SOLID45 is used for the 3-D modeling of solid structures.

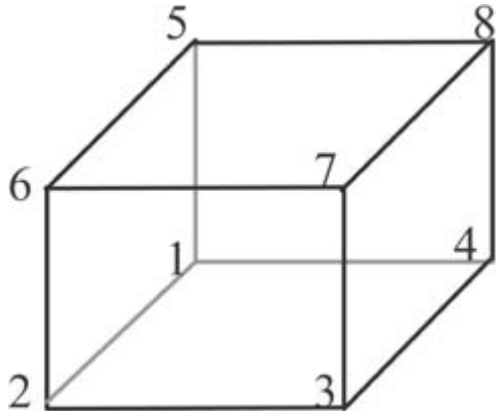

Figure 4.1 Three-dimension cubic element

The element is defined by eight nodes having three degrees of freedom at each node: translations in the nodal x, y, and z directions. The element has plasticity, creep, swelling, stress deflection, and large strain capabilities. A higher-order version of the SOLID45 element is SOLID95.

The prototype used is of dimensions as shown in **Figure 4.2**.There are 1050 elements and 1408 nodes in this work. The properties of the liquid mesh have no cure characteristics before it has been determined to be exposed according to the mask pattern or the laser path planning drawing. The cured elements of the current layer are constructed as a global stiffness matrix. The boundary condition is then recombined and saved as a nodal displacement vector.

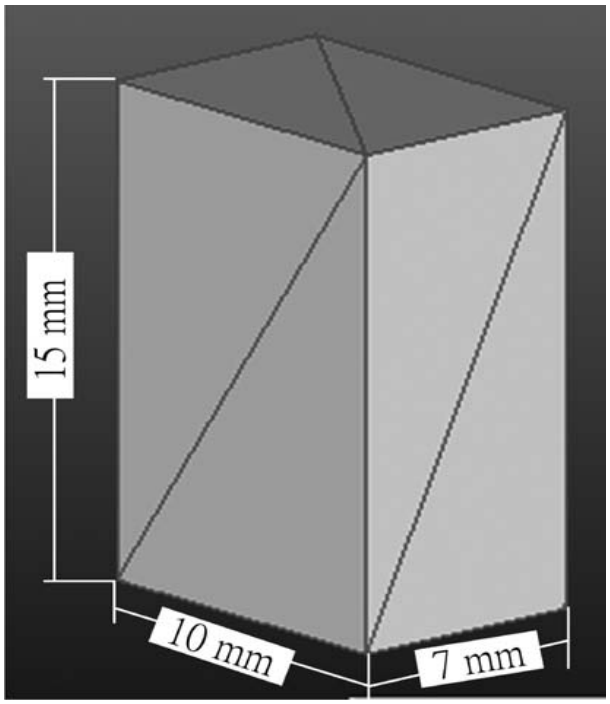

Figure 4.2 Prototype of cubic solid

Hence, the shrinkage and internal stress starts the calculation. If the next layer is checked and it is determined that it needs to be fabricated, than the previous process is repeated until no more layers need to be fabricated.

4.2 FLOWCHART OF SIMULATION PROCESS:-

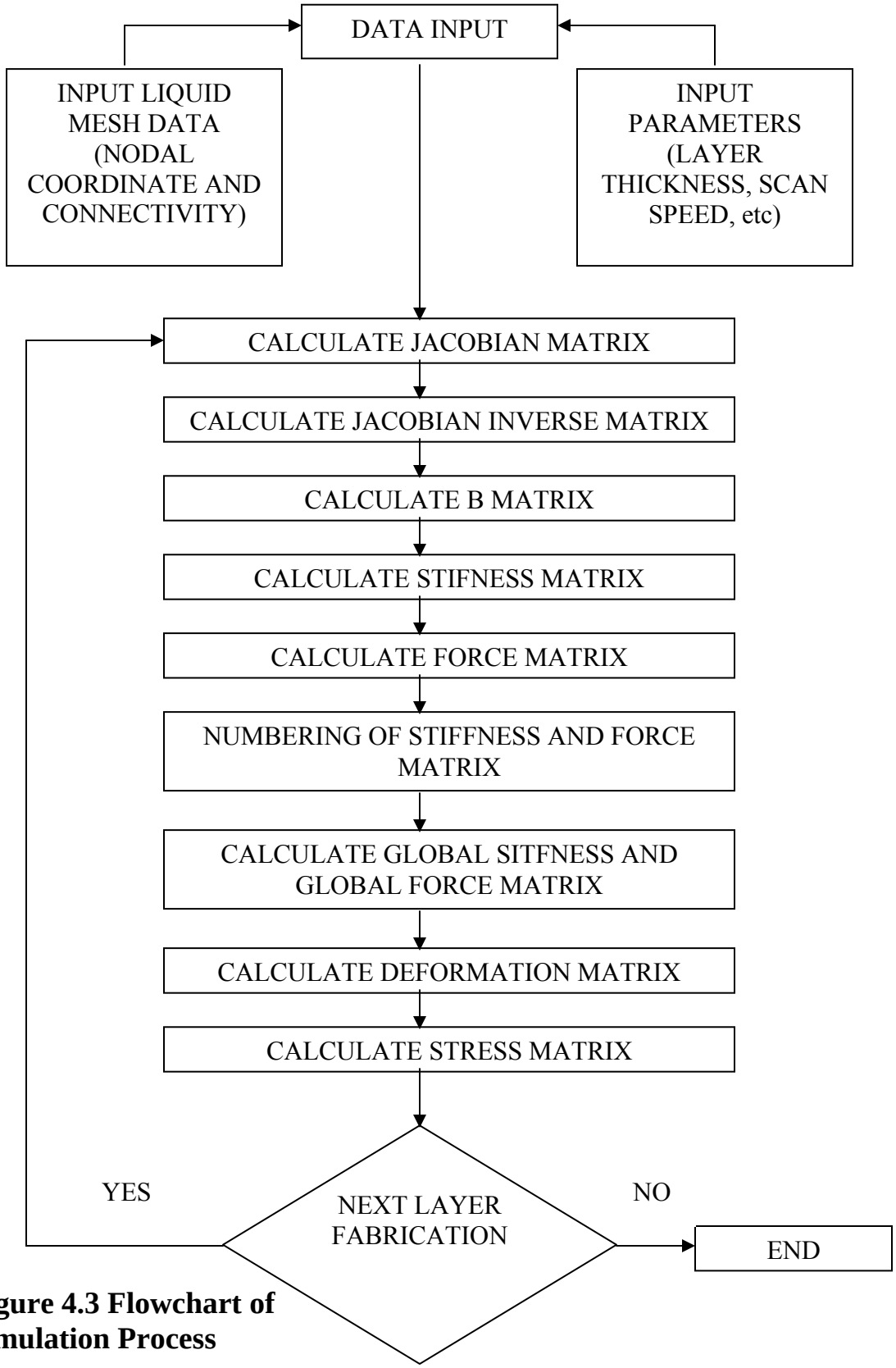

Figure 4.3 Flowchart of Simulation Process

CHAPTER-5 RESULTS AND DISCUSSIONS

In respect to the procedure followed the basic finite element steps are applied and the following findings are seen which are:

- Discretization or mesh generation: The dimensions of prototype taken are 10*7*15 cubic mm. The model of the prototype is made and meshed in ANSYS software. It is meshed into 1050 element and 1408 nodes. The element type taken is SOLID 45. The element is defined by eight nodes having three degrees of freedom at each node: translations in the nodal x, y, and z directions. and following results are obtained which are shown in following Figures:

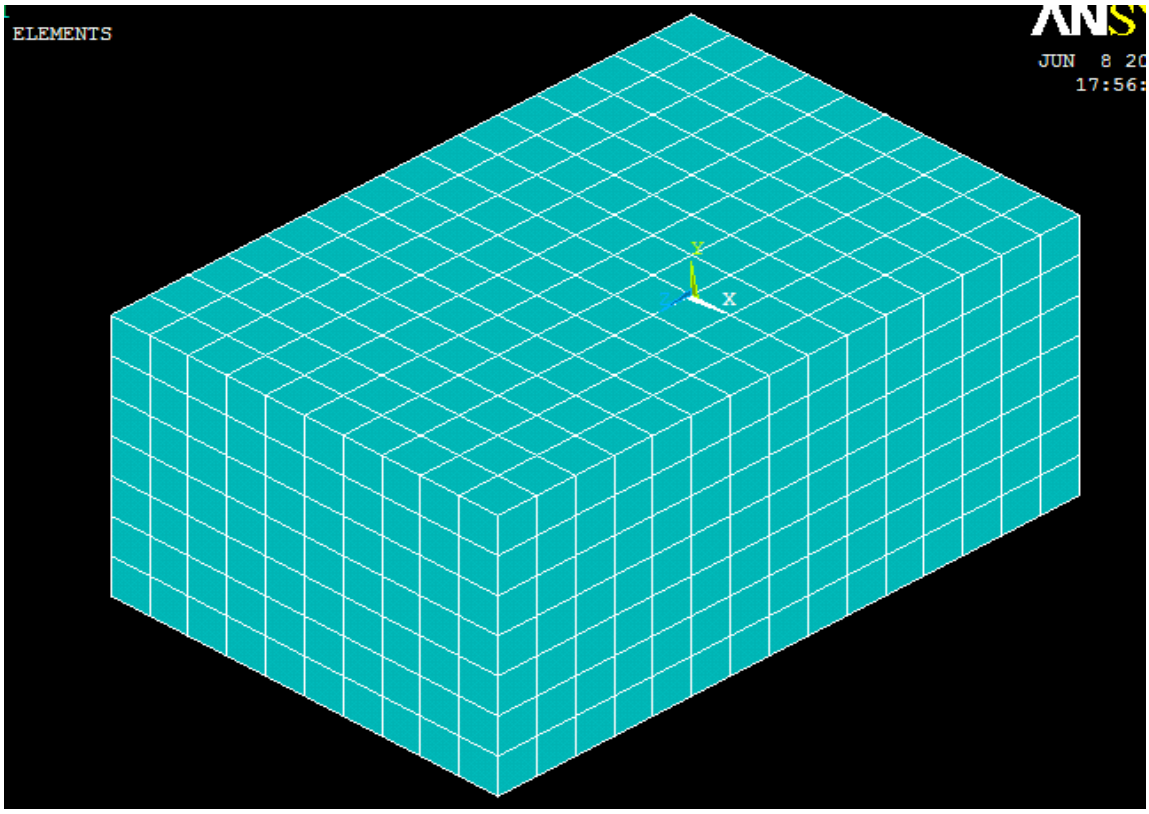

Figure5.1 Meshed part

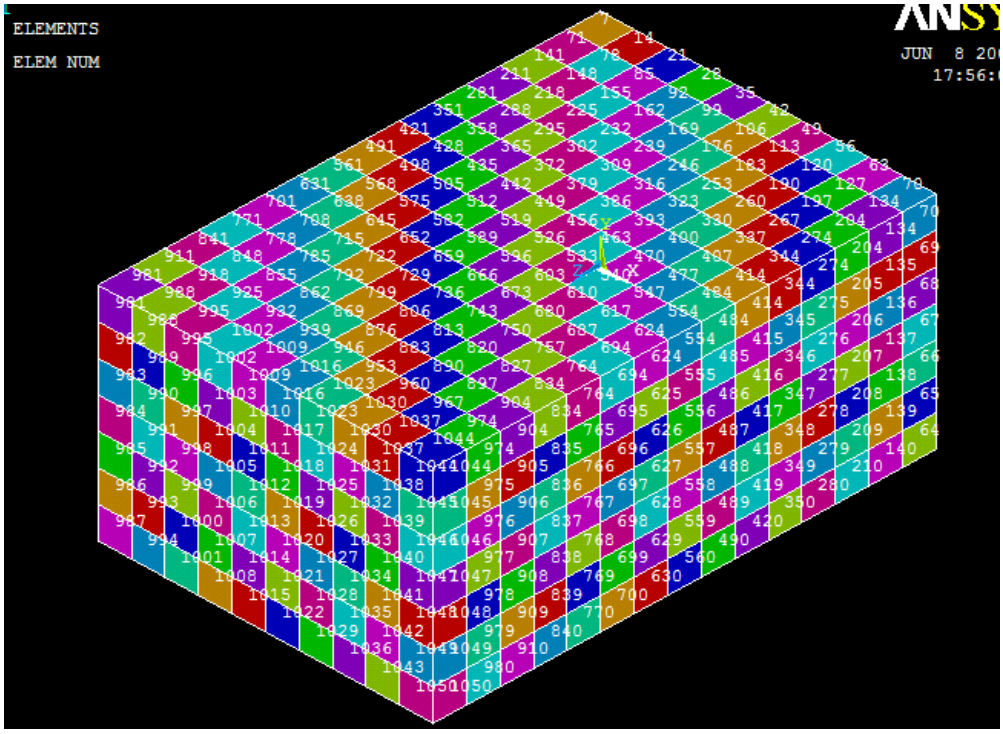

Figure5.2 Meshed part with numbering

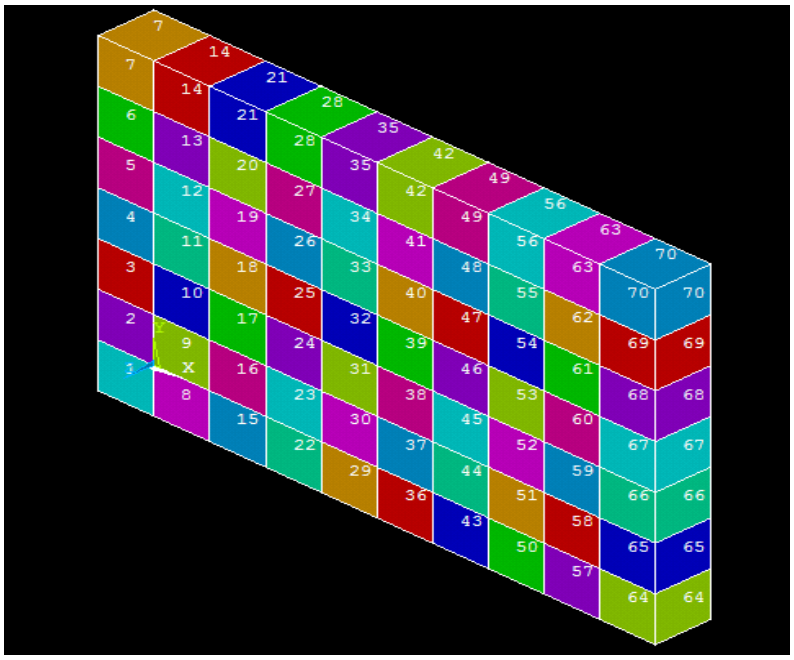

Figure5.3 LAYER-1

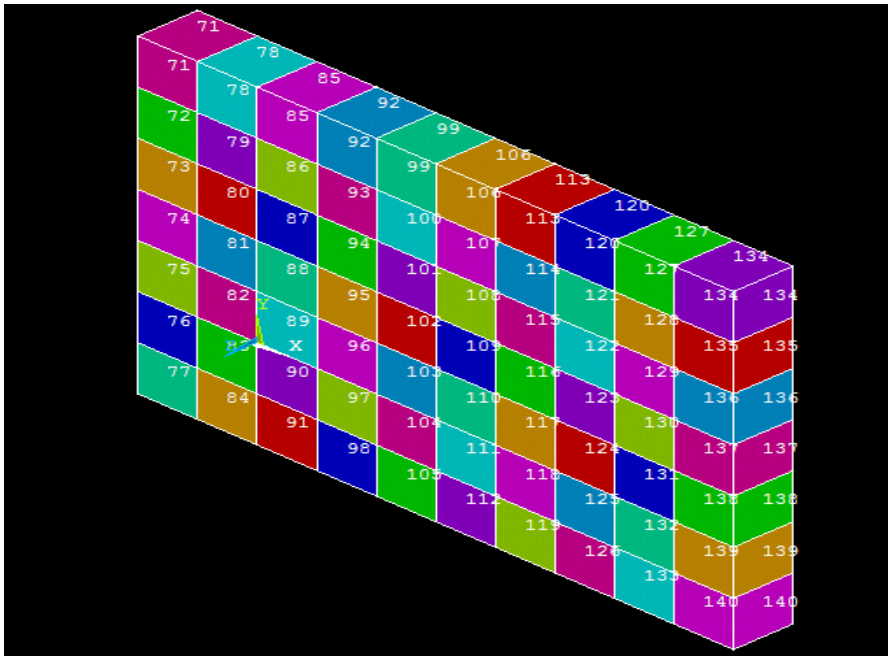

Figure5.4 LAYER-2

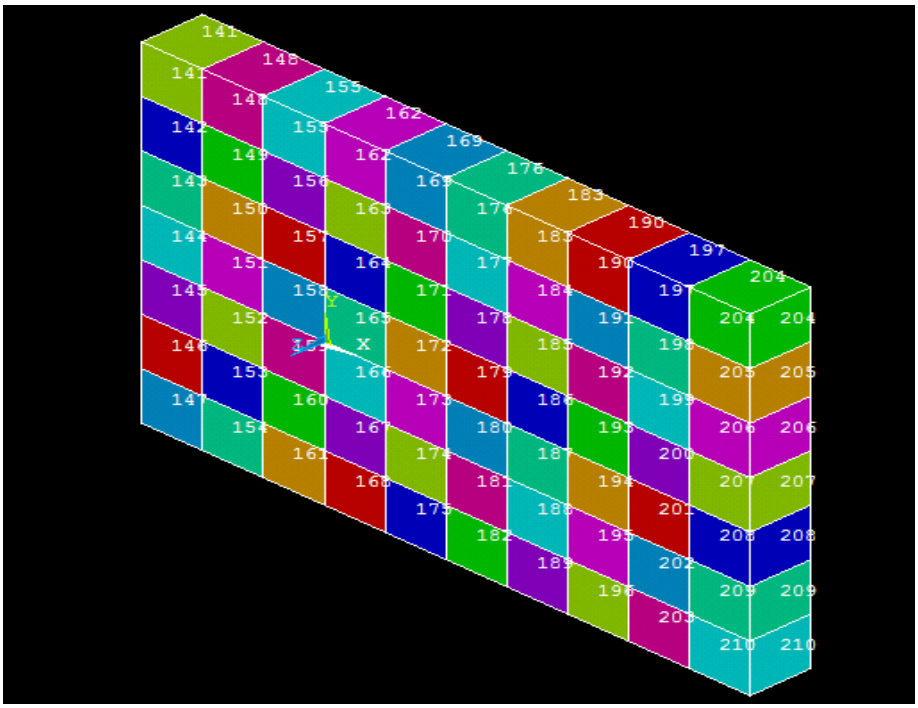

Figure5.5 LAYER-3

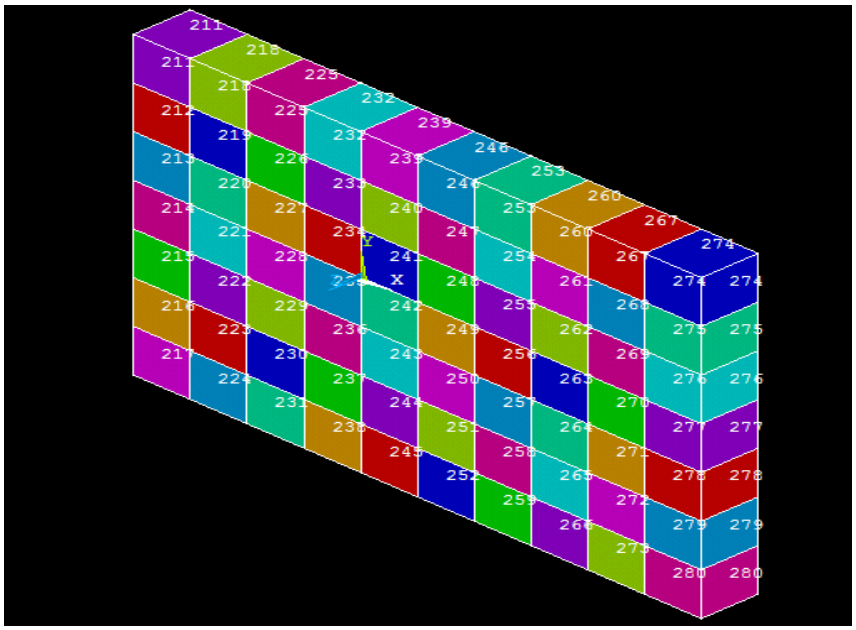

Figure5.6 LAYER-4

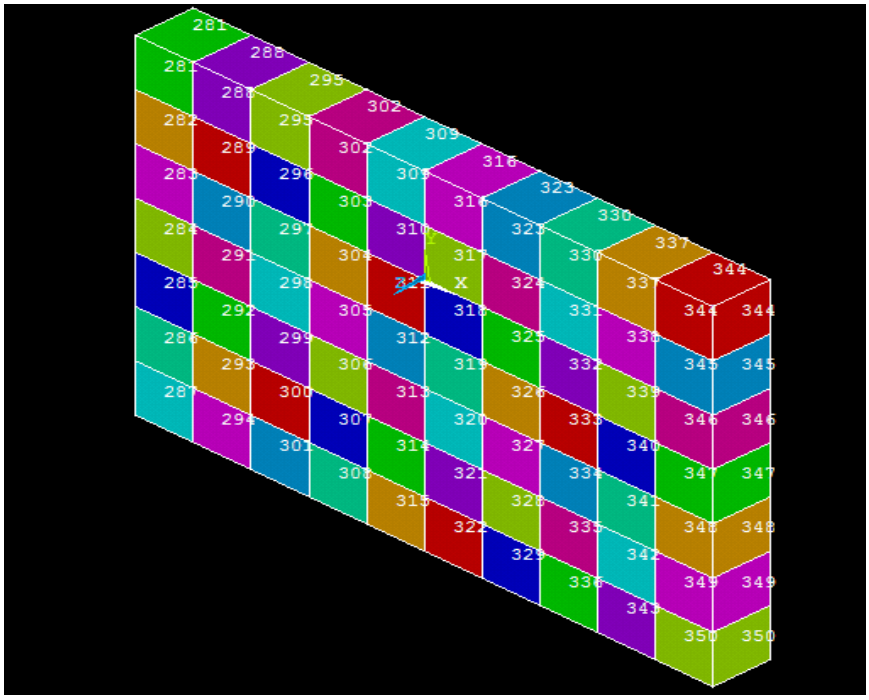

Figure5.7 LAYER-5

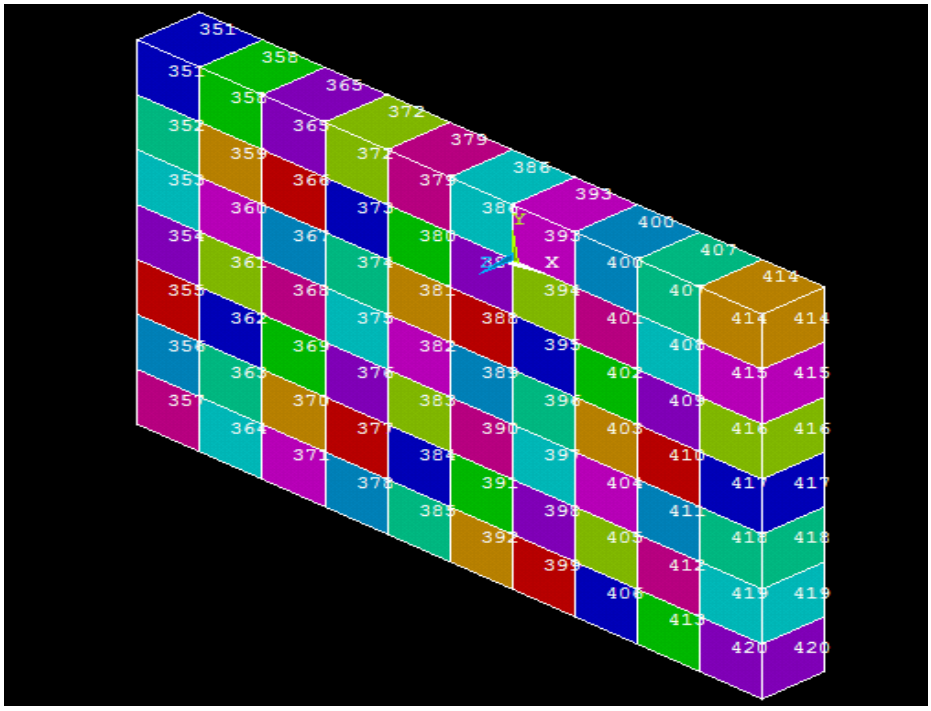

Figure5.8 LAYER-6

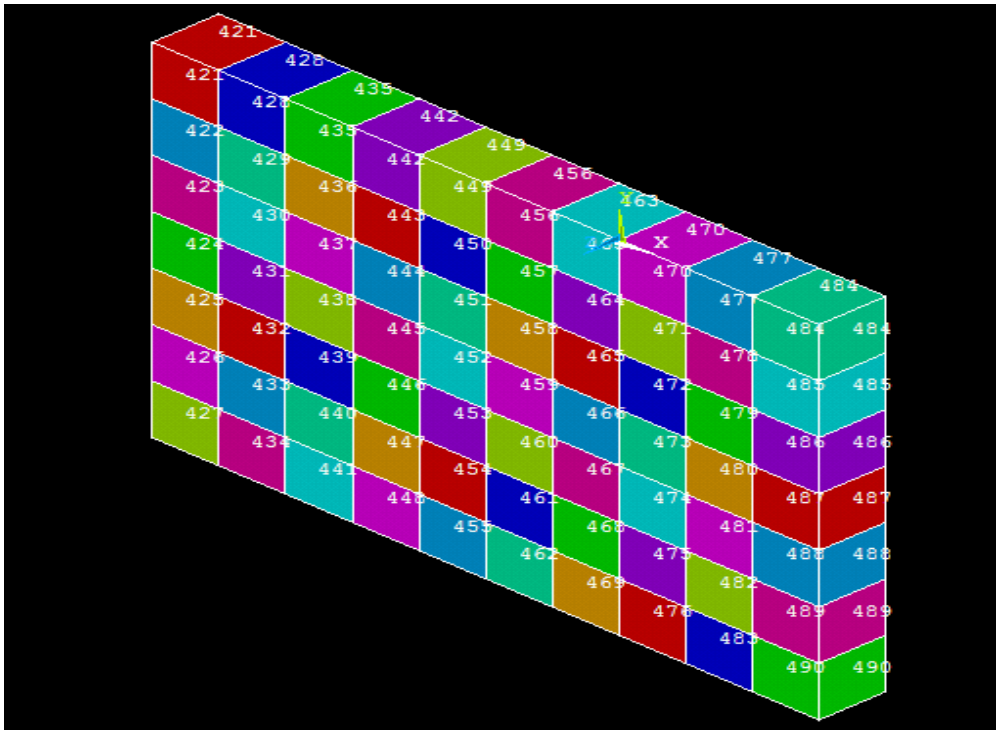

Figure5.9 LAYER-7

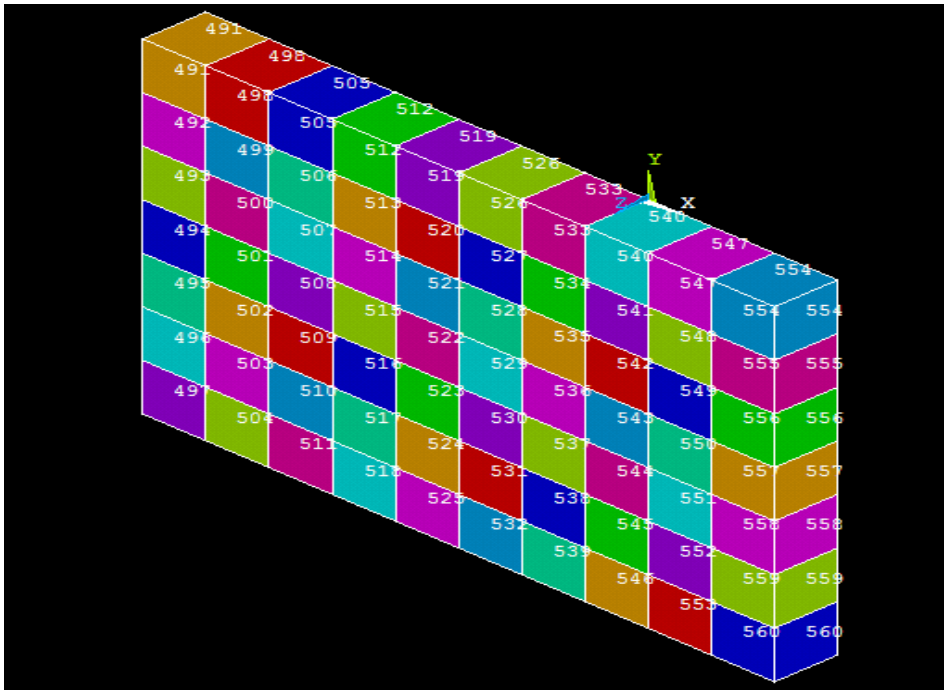

Figure5.10 LAYER-8

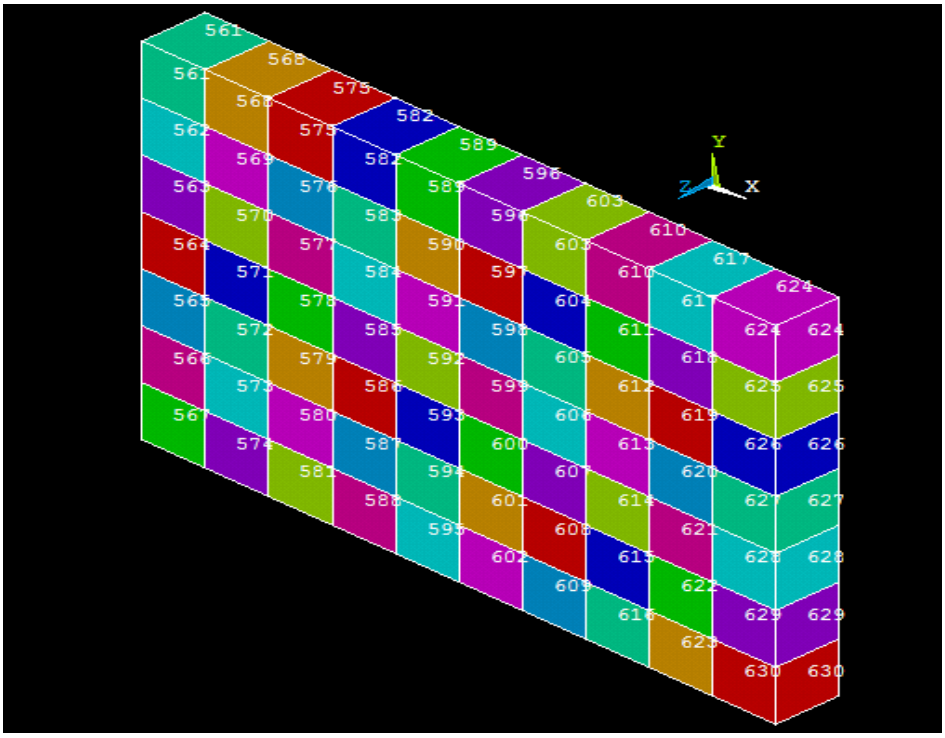

Figure5.11 LAYER-9

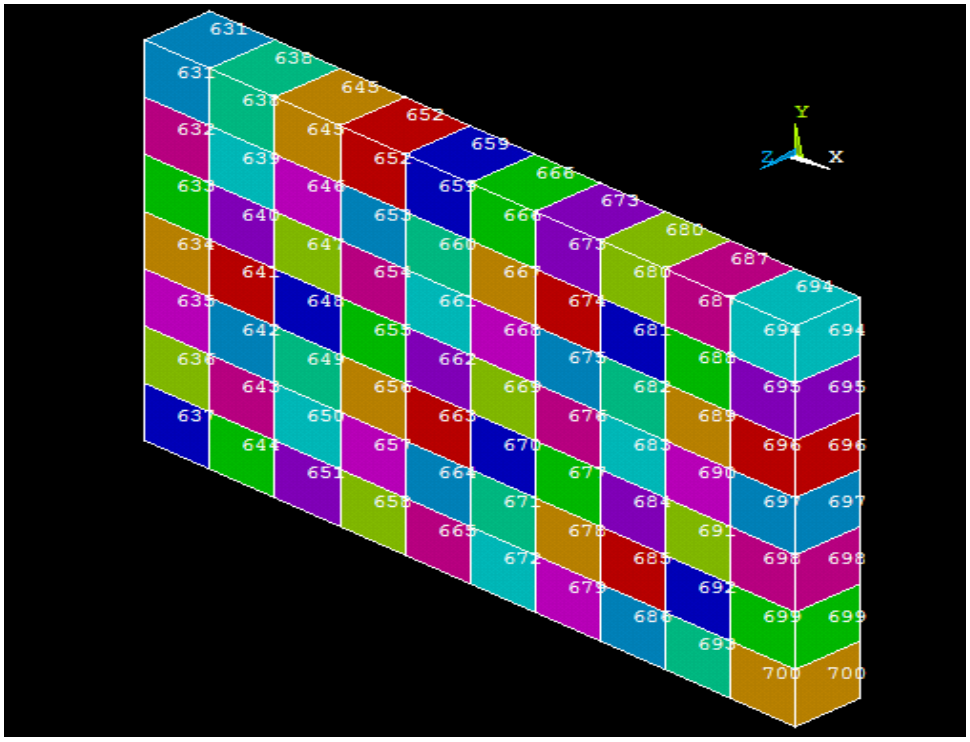

Figure5.12 LAYER-10

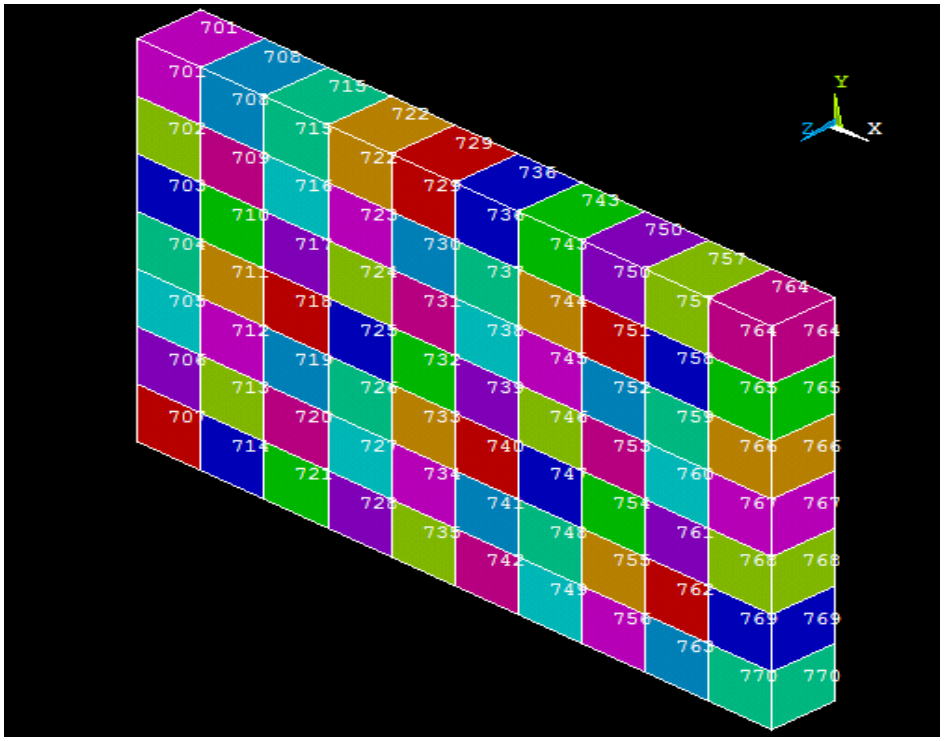

Figure5.13 LAYER-11

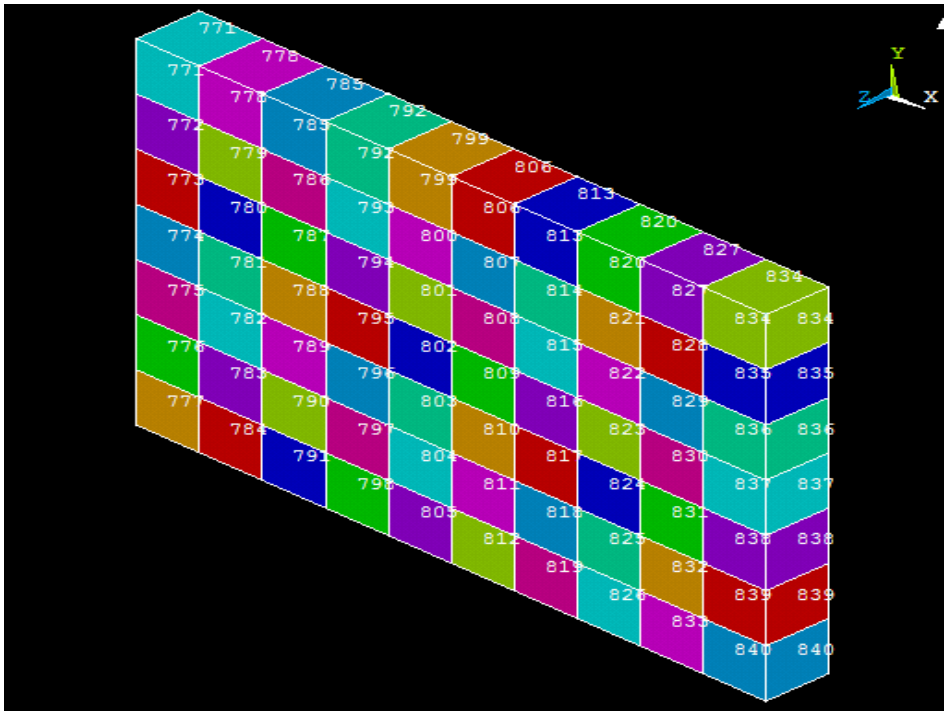

Figure5.14 LAYER-12

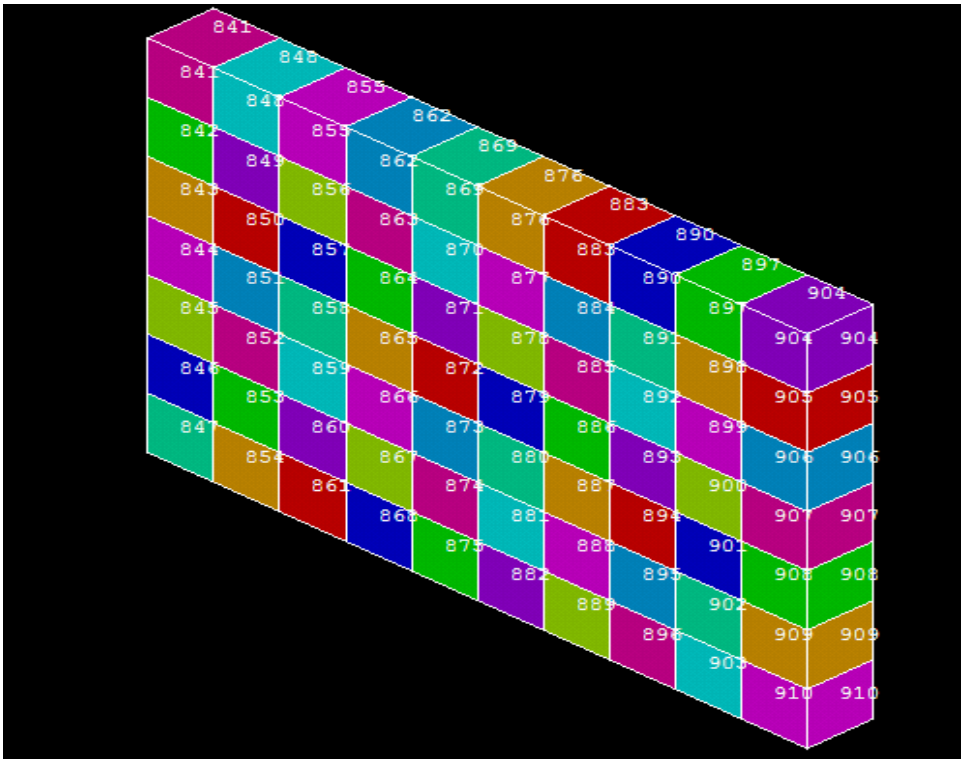

Figure5.15 LAYER-13

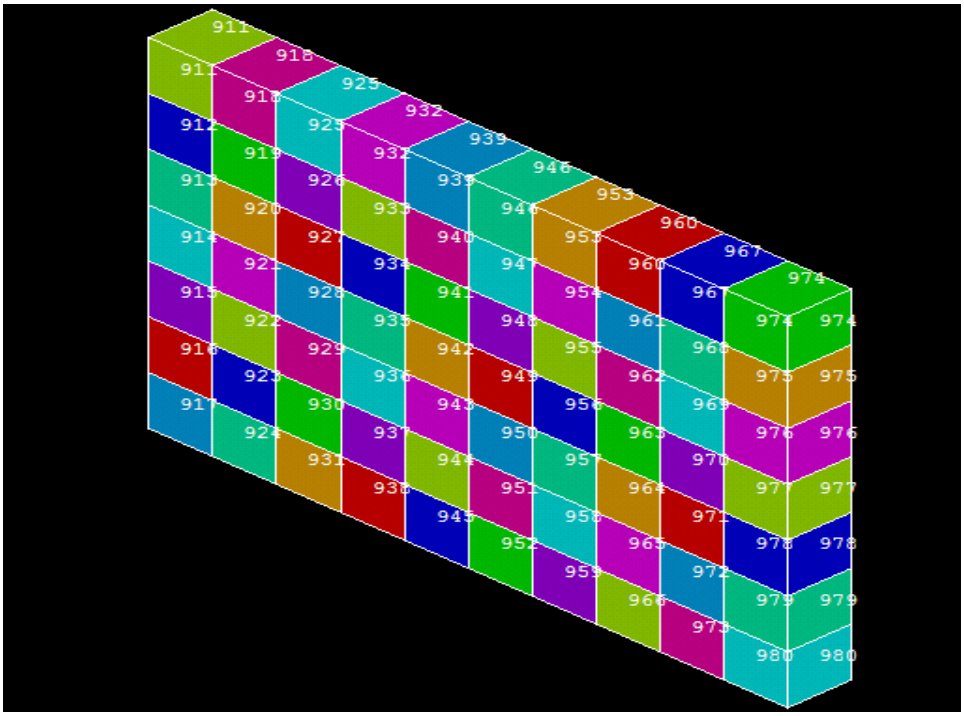

Figure5.16 LAYER-14

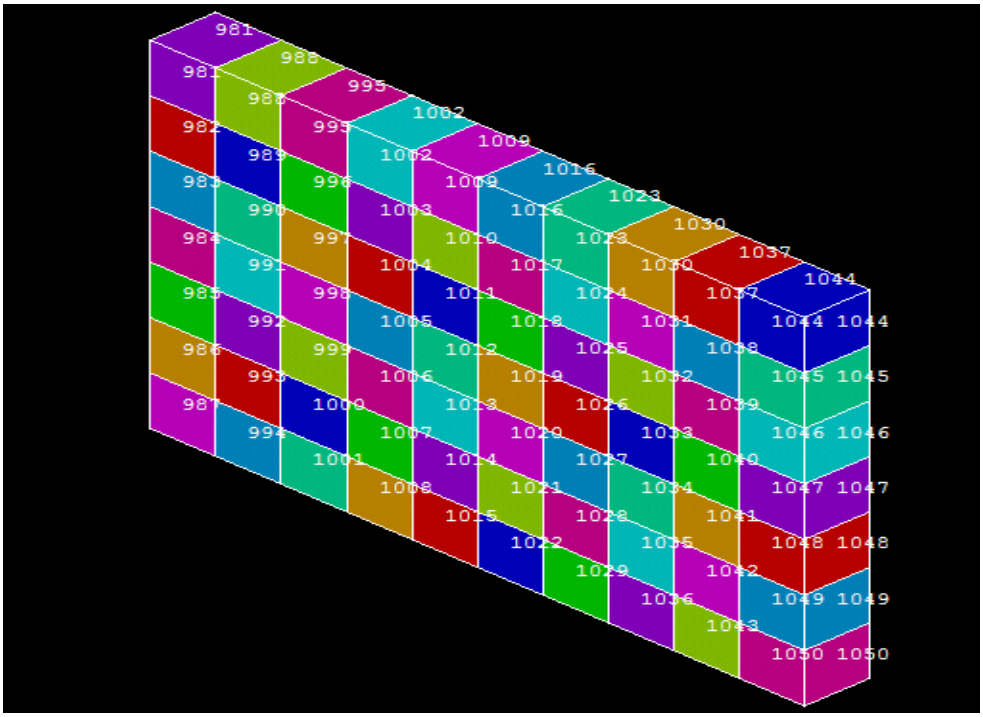

Figure5.17 LAYER-15

- Generate element stiffness matrix: The element stiffness matrix which must be of the order of $[24*24]$ is successfully generated which is in accordance with the formula:

$$[k] = \int_v [B]^T [D^e][B] dV \qquad \textbf{(5.1)}$$

where K represents the element stiffness matrix;

B represents the strain rate–velocity matrix of order $[6*24]$;

D represents the stress-strain matrix of order $[6*6]$;

t represents the thickness;

det J represents the determinant of Jacobian matrix of order $[3*3]$;

- System stiffness matrix or Overall stiffness matrix or global stiffness matrix:

Before generating the global stiffness matrix the numbering scheme for each node using 3n-2, 3n-1,3n sequence is done successfully to assemble all element stiffness matrices in global stiffness matrix of the order of $[4224*4224]$. This order is in conformance to numbering scheme used which implies that as the maximum node number is 1408, so if the numbering scheme is applied than the highest order must be of $[4224*4224]$. Thus global element stiffness matrix of this order is generated. And similarly global force matrix of the order $[4224*1]$ is also generated using formula:

$$\{\dot{F}\} = \int_v \left[[B]^T \{\sigma\} - [B]^T (3k) \{\alpha \dot{T} + \Delta\beta(I)\} \right] dV \qquad \textbf{(5.2)}$$

- Boundary conditions or loading conditions: Then the boundary conditions are also successfully applied.

- Solving the matrix : To get the distortion data the displacement matrix signifying displacement of each node is generated using formula:

$$[Kglobal][u]-[Fglobal]=0 \quad \textbf{(5.3)}$$

where $[Kglobal]$ is the global stiffness matrix;

$[Fglobal]$ is the force matrix;

$[u]$ is the displacement matrix;

Thus displacement matrix of the order $[4224*1]$ is generated which gives the distortion data. After this the stress are found out for each element using the formula:

$$\{\dot{\sigma}\}=\left[D^{e}\right]\{\dot{\varepsilon}\}-3k\{\alpha\dot{T}\}-\{\sigma(t)\}-3k\{\Delta\beta(I)\} \quad \textbf{(5.4)}$$

where $$\{\dot{\varepsilon}\}=[B]\{\dot{u}\} \quad \textbf{(5.5)}$$

and $\{\dot{\sigma}\}$ represents the stress

in which $\{\dot{u}\}$ is the increment in nodal displacement which was found in above step.

- Display: Finally the distortion data and the stress values as generated are displayed.

CHAPTER-6 CONCLUSION AND FUTURE SCOPE

6.1 CONCLUSION:

In this work, stereolithography modeling simulations in a cubic part are studied. A finite element method for the simulation of the liquid stereolithography process is employed to find the distortion caused by shrinkage during the photopolymerization process. From this work it is see that the major problem of distortion in sterolithography process must be tackled before the actual manufacturing so that the manufacturer come to know about the discrepancies to be handled in advance so that the accuracy and precision could be maintained and improved.. This not only saves time but also reduce the losses and will create benefits for the firm and for research.

6.2 FUTURE SCOPE:

1. This work focuses on the development and application of CAE simulation code in the RP fabrication, which not only successfully employs a finite element method to simulate distortion but can also be used to obtain a higher precision on the final parts through compensation of the original CAD model before build-up prototyping.
2. By using the proposed method in the present study, manufacturers can use lower-cost machines to obtain a higher precision on final-parts, or obtain a more accurate precision on the same machines.
3. Manufacturers can use the method in this study to avoid building a support for with a bending stress. However, the part is more accurately produced, reducing the time required for post-processing.
4. By using the method in this study, manufacturers can use simple laser scan path planning to obtain a higher precision on final-parts.
5. It is believed that this research method can be promoted to other materials or build methods in RP fabrication, so as to acquire a more accurate precision on final-parts, and further increase the application of RP in various industrial scopes.
6. The results can be further applied to micro RP, so as to obtain more accurate precision and prototypes.
7. The work can be applied to any geometric part as long as the finite element mesh can be created, but it is not limited to simple parts. As to the fabrication of the reverse

compensation CAD model in much more complex parts, it can be divided into many simple cells and then the new CAD model can be assembled by each simple cell finished.

Finally this work can be used in finding %error in the actual dimensions of the part to be build and a reverse compensation process can be applied to remove such error to increase the accuracy and precision.

CHAPTER-7 REFERANCES

[1] P.F. Jacobs, "Rapid Prototyping and Manufacturing Fundamentals of Stereolithography", ASME Press, New York, (1992).

[2] Gabriel Bugeda, Miguel Cervera, Guillermo Lombera and Eugenio Onate, "Numerical analysis of stereolithography processes using the finite element method", Rapid Prototyping Journal, Vol.1 (2), pp.12–23(1995).

[3] R.S.Chambers, T.R.Guess and T.D.Hinnerrichs, "A Phenomological Finite Element Model of Part Building in Sterolithography Process", Sixth International Conference on Rapid Prototyping, Dayton, Ohio, June 4-7(1995).

[4] B. Wiedemann,K. H. Duseland J. Eschl, "Investigation into the influence of material and process on part Distortion", Rapid Prototyping Journal, Vol.1, Number 3, pp. 17–22(1995).

[5] T.R.Guess and R.S.Chambers, "In-Situ Property Measurements On Laser-Drawn Strands Of SL 5170 EPOXY AND SL 5149 ACRYLATE", The Sixth Solid Freeform Fabrication Symposium, Austria, August 7-9(1995).

[6] Hiroyuki Narahara, Fumiki Tanaka, Takeshi Kishinami, Satoru Igarashi and Katsumasa Saito, "Reaction heat effects on initial linear shrinkage and deformation in stereolithography", Rapid Prototyping Journal, Vol.5 (3), 120–128(1999).

[7] H.S. Cho, W.S. Park, "Determining optimal parameters for stereolithography processes via genetic algorithm", Journal of Manufacturing Systems, Vol.19 (1), pp.18–34(2000).

[8] W. L. Yao and Ming C. Leu, "Analysis and design of internal web structure of laser stereolithography patterns for investment casting", Materials & Design Vol.21, Issue 2, pp. 101-109(2000).

[9] S H Lee, W S Park, H S Cho, W Zhang and **M C Leu ,** "A neural network approach to the modelling and analysis of stereolithography processes" Proc. Instn. Mechanical Engineers, Vol.215 Part B (2000).

[10] S. S. Hur, J. R. Youn, "Thermal Deformation of a Photo-Cured Polymer for the Analysis of Sterolithography**",** Polymer–Plastic Technology Engineering, Vol.39 (4), pp 651–666(2000).

[11] Y.M. Huang, "Computer supported force analysis and layer imagine for masked rapid prototyping system", in Proceedings of the 6th International Conference on Computer Supported Cooperative Work in Design, Ontario, Canada, pp. 562–567(2001).

[12] D. Karalekas, D. Rapti, E. E. Gdoutos, and A. Aggelopoulos, "Investigation of Shrinkage-induced Stresses in Stereolithography Photo-curable Resins", Experimental Mechanics, Vol.42, No. 4(2002).

[13] Y.M. Huang, C.P. Jiang, "Curl distortion analysis during photopolymerization of stereolithography using dynamic finite element method**",** International Journal of Advance Manufacturing Technology, Vol.21, pp.586–595(2003).

[14] Y.M. Huang, C.P. Jiang, "Numerical analysis of mask type stereolithography process using dynamic finite element method", International Journal of Advance Manufacturing Technology, Vol.21 , pp. 649–655(2003).

[15] Y.M. Huang, J.Y. Jeng, C.P. Jiang, J.C. Wang, "Increased accuracy by using dynamic finite element method in the constrain–surface stereolithography system", Journal of Material Processing Technology, Vol.140, pp. 191–196(2003).

[16] J.D. Curtis, S.D. Hanna, E.A. Patterson and M. Taroni, "On the Use of Stereolithography for the Manufacture of Photoelastic Models", Society for Experimental Mechanics, Vol.43, No. 2(2003).

17 Jeffrey Stansbury and Junhao Ge, "Photopolymerization Shrinkage and Stress in Resins and Composites", Radtech Report (2003).

[18] Y.-M. Huang, S. Kuriyama, C.P. Jiang, "Fundamental study and theoretical analysis in a constrained-surface stereolithography system", International Journal of Advanced Manufacturing Technology Vol.24, pp.361–369(2004).

[19] R. Hague, S. Mansour, N. Saleh, R. Harris, "Materials analysis of stereolithography resins for use in Rapid Manufacturing," Journal Of Materials Science, Vol.39, pp.2457 – 2464(2004).

[20] Wenbin Hong, Yong Tsui Lee, Haiqing Gong, "Thermal analysis of layer formation in a stepless rapid prototyping process", Applied Thermal Engineering Vol.24, pp.255–268(2004).

[21]Y.M. Huang, H.Y. Lan, "CAD/CAE/CAM integration for increasing the accuracy of mask rapid prototyping system", Computers in Industry, Vol.56, pp.442–45(2005).

[22] You-Min Huang and Hsiang-Yao Lan, "Dynamic reverse compensation to increase the accuracy of the rapid prototyping system", Journal of Materials Processing Technology Vol.167, Issues 2-3, pp.167-176(2005).

[23] You-Min Huang, Hsiang-Yao Lan, "Compensation of distortion in the bottom exposure of stereolithography process", International Journal of Advanced Manufacturing Technology Vol.27, pp. 1101–1112(2006).

[24] Cho-Pei Jiang, You-Min Huang and Chun-Ho Liu, "Dynamic finite element analysis of photopolymerization in stereolithography", Rapid Prototyping Journal, Vol. 12, Number 3, pp. 173–180(2006).

[25] Yuung-Hwa Lu, "Integration of RP and explicit dynamic FEM for the visualization of the sheet metal forming process", International Journal Advanced Manufacturing Technology Vol.28, pp. 255–261(2006).

[26] K. Chockalingam, N. Jawahar, K.N. Ramanathan · P.S. Banerjee, "Optimization of stereolithography process parameters for part strength using design of experiments", International Journal Advanced Manufacturing Technology Vol. 29, pp.79–88(2006).

[27] You-Min Huang, Hsiang-Yao Lan, " Path planning effect for the accuracy of rapid prototyping system", International Journal Advanced Manufacturing Technology Vol.30, pp.233–246(2006).

[28] D.E. Karalekas, A. Agelopoulos, "On the use of stereolithography built photoelastic models for stress analysis investigations", Materials and Design Volume Vol.27, pp.100–106(2006).

[29] Fernand Ellyin, Zihui Xia, "Nonlinear Viscoelastic Constitutive Model for Thermoset Polymers" Journal of Engineering Materials and Technology, Vol.128, pp. 579-585(2006).

[30] Jae-Hyung Sim, Eun-Dok Lee and Hyeog-Jun Kweon, "Effect of the Laser Beam Size on the Cure Properties of a Photopolymer in Stereolithography", International Journal of Precision Engineering and Manufacturing, Vol. 8, No.4, pp.50-55(2007).

.